Geotextiles and Geomembranes 53 (2025) 277–294

Contents lists available at ScienceDirect

Geotextiles and Geomembranes

journal homepage: www.elsevier.com/locate/geotexmem

Regular Paper

Effect of backfilling surface settlement trough on waste cover leakage

Y.H. Fan, R. Kerry Rowe *, Richard W.I. Brachman, Jamie F. VanGulck

GeoEngineering Centre at Queen's-RMC, Dept. of Civil Engineering, Queen's Univ., Kingston, ON, Canada, K7L 3N6

ARTICLE INFO

Keywords:
Geosynthetics
Geomembrane
Leakage
Hole
Repair
Differential settlement

ABSTRACT

The effect of backfilling of a surface differential settlement trough to reduce leakage is explored both experimentally and numerically. The field experiment examined two lined sections each with an 11 mm-diameter hole in the liner on a nominally 4 horizontal:1 vertical slope. A 2 m by 3 m, 0.3 m deep depression was filled with a 50-50 sand-snow mixture in winter to give a continuous 4H:1V slope prior to covering with the liner and 0.3 m of cover soil. Spring thaw induced a differential settlement trough up to 0.14 m deep. A second section with a similar trough was backfilled with cover soil to reinstate the 4H:1V surface while the settlement depression in the liner remained. Over the 15 months of monitoring, the backfilling reduced leakage by 57% from a annual total of 565 L to 244 L (i.e., a 60% reduction in colder seasons, from 351.3 L to 137.8 L together with a 45% reduction in warmer seasons, from 141.8 L to 77.6 L). A 3D numerical model showed encouraging agreement with the experimental results. The model indicated an inverse relationship between leakage and slope gradient, and a direct relationship between leakage and depression depth and upgradient distance to the depression. The effect of cover hydraulic conductivity was complex.

1. Introduction

A 1.5 to 2 mm-thick geomembrane (GMB) liner in waste covers is an effective component to minimize seepage from rain and snow into waste (Rowe et al., 2004). However, the occurrence of GMB holes is a well-documented issue (Brachman and Eastman, 2013; Eldesouky and Brachman, 2018; Gilson-Beck, 2019). It is generally assumed that a well-installed GMB will have about 2.5–5 holes per hectare (Giroud, 2016; Giroud and Bonaparte, 1989, 2001; Rowe, 1998, 2005, 2012, 2020), although for mining covers in the North, this number can easily go to about 20 holes per hectare (H. Bremner et al., 2016). These holes can lead to leakage into the waste (Fig. 1a), consequently elevating leachate head above GMB liners and increasing the risk of environmental contamination (Zhang et al., 2021).

Extensive research has been conducted on leakage through GMB liners (Brachman et al., 2017; Giroud, 2016; Pandey and Shukla, 2020; Ramasamy et al., 2018; Rowe and Abdelatty, 2013; Rowe and Fan, 2021; Rowe et al., 2017b; Touze-Foltz et al., 2021; Xie et al., 2023; Xu et al., 2018) but the impact of differential settlement on a waste cover slope is rarely discussed. Differential settlement can arise in many ways. For instance, the leakage through a hole can result in depression (i.e., differential settlement) (Fig. 1b), because

(i) leakage through GMB holes may induce erosion or piping of subgrade due to washout of fine particles (Fan and Rowe, 2022; Stohr et al., 1988), and
(ii) the warm fluid through holes in the winter or spring season can induce the melt of frozen subgrade or waste, which aggravates differential settlement.

Differential settlement in waste covers can also occur before the formation of GMB holes because of the uneven degradation/settlement of the waste underneath and melting of frozen waste and/or subgrade (McDougall et al., 2018; Zhu). As a result, the strain induced by differential settlement could lead to defects/holes in GMB due to stress cracking in the long term (Fan et al., 2021; Rowe and Yu, 2019), which increases the differential settlement (Fig. 1 b). This detrimental cycle emphasizes the significance of quantifying the leakage through a hole/defect that can be caused due to differential settlement.

Given the strong influence of field climatic factors like temperature and rainfall on leakage (Williams, 2008), Fan et al. (2024) conducted field experiments with Sections A and B on a slope to simulate waste covers and showed the leakage through an 11 mm-diameter hole in GMB can be increased by 50-fold due to a 3 m × 2 m × 0.12–0.17 m depression in Section B compared to Section A without a depression. This finding confirmed the significant effect of differential settlement on

* Corresponding author.
E-mail addresses: fan.y@queensu.ca (Y.H. Fan), kerry.rowe@queensu.ca (R.K. Rowe), richard.brachman@queensu.ca (R.W.I. Brachman), jamie.vangulck@queensu.ca (J.F. VanGulck).

https://doi.org/10.1016/j.geotexmem.2024.09.010
Received 10 June 2024; Received in revised form 31 July 2024; Accepted 15 September 2024
Available online 5 October 2024

Notation;

VWC_0	Initial volumetric water content of the cover soil (dimensionless)
VWC	Volumetric water content of the cover soil (dimensionless)
k	Hydraulic conductivity of the cover soil (m/s)
k_{ref}	Hydraulic conductivity of the saturated cover soil at the reference temperature (21.9 °C) (m/s)
k_T	Hydraulic conductivity of the saturated cover soil at the measured soil temperature (m/s)
k_{local}	Hydraulic conductivity of the saturated soil within the 5-cm region from the hole (m/s)
k_{global}	Hydraulic conductivity of the saturated soil everywhere except for the region within 5 cm (m/s)
μ_{ref}	Viscosity of water at the reference temperature in the laboratory (21.9°C) (mPa·s)
μ_T	Viscosity of water at the soil temperature measured in the field (mPa·s)
d_{10}	The particle diameter at which 10% of the mass is finer (mm)

ABBREVIATIONS

GMB	Geomembrane
HDPE	High-density polyethylene
QUELTS	The Queen's University Environmental Liner Test Site
2D	Two dimensional
3D	Three dimensional

leakage but did not address the potential effect of repair. A case study by Scalia et al. (2017) showed a repair approach that included removing cover materials to the subgrade, repairing the soil barrier, installing new geosynthetics, and replacing the overlying earthen cover materials according to design specifications. This approach, though potentially effective, is time-consuming and costly, making it particularly challenging for cold regions with permafrost (Buslaev et al., 2021; Subbotin et al., 2022) or remote regions with limited/restricted access to equipment (Keske et al., 2018), and for waste facilities with radioactive waste with health hazards (Butler, 2002; Nyhan, 2005). As an alternative, a potential cost-efficient approach is repairing by filling the surface trough without excavating once a trigger depth of trough is reached (Fig. 1c). This approach is widely practiced for maintaining and repairing pavement, and the leakage is likely to be reduced, but the quantification of the effect is needed. Thus, a new field experiment section, Section C, which features an identical depression beneath the GMB as Section B but with the surface trough repaired is needed. This new section aims to quantify the effect of filling the surface trough so that this approach can be evaluated for waste cover maintenance and repair.

Fan et al. (2024) observed that Section B, a waste cover slope (4H:1V) with a depression (0.12–0.17 m deep), experienced 281 L of leakage following 284 mm of precipitation between November 2022 and February 2023, whereas only 142 L of leakage from 537 mm of precipitation between June and September 2022. The pattern of increased leakage during colder temperatures aligns with the observations of seasonal soil moisture variations reported by Weeks and Wilson (2005). This observation can be attributed to the less evaporation, and counterintuitively, the lower hydraulic conductivity which is sensitive to the temperature-dependent viscosity (Hopmans and Dane, 1986). The leakage decreases with lower hydraulic conductivity due to increased resistance to downslope flow and prolonged water head above the hole (Fan et al., 2024). While this finding is significant, the relationship between different typical hydraulic conductivities of sand material and leakage remains unquantified. Moreover, the previous experiment

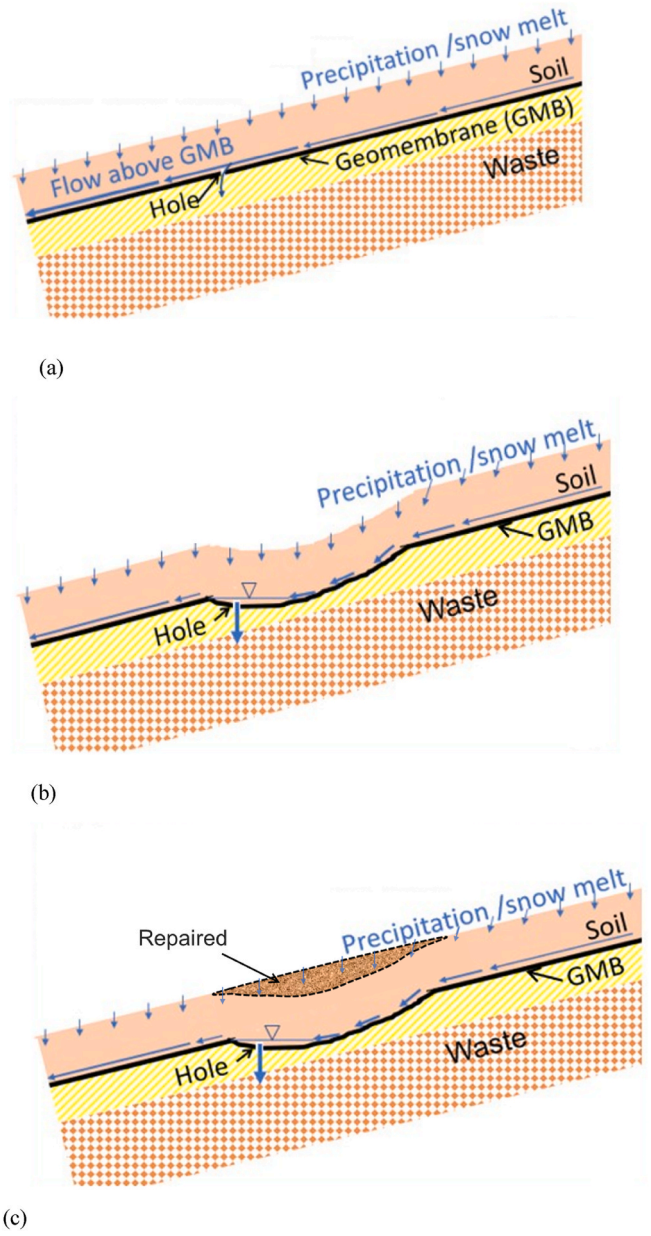

Fig. 1. Schematic showing (a) the scenario with a hole in the geomembrane of very limited leakage on a 4H:1V slope; (b) the notable increase in leakage that occurs with differential settlement; (c) surface trough being repaired and relevelled

placed the GMB hole 300 mm from the depression's bottom contour; however, strain could position the hole at the lowest contour, leaving the impact of hole locations unexplored. Additionally, the results from specific geometry (cover thickness, depression depth) in the experiment may not be applicable to wider waste cover scenarios, necessitating parametric studies to provide more generalized design guidance for waste covers under various field conditions.

The first objective of this paper is to quantify how much leakage through a GMB hole can be reduced by repairing (filling) a surface trough on a 4H:1V slope. This quantification will provide insights to cost-effective strategies for mitigating differential settlement in waste covers. The second objective is to calibrate numerical models with field data so that parametric studies can be conducted to investigate the effect of hydraulic conductivity, depth and location of differential settlement, location of GMB holes, and the gradient of the slope. These numerical results will broaden the applicability of leakage prediction to various

waste cover designs, providing practical guidance for designing effective waste covers from the perspective of leakage control.

2. Field experiment

2.1. Location and design

The field experiments for this study were conducted at the Queen's University Environmental Liner Test Site (QUELTS), located 40 km northwest of Kingston, Ontario, Canada, at coordinates 44°34′N and 76°39′W. In preparation for the field test, a thorough survey was conducted, resulting in the selection of a south-facing slope area measuring approximately 8 m wide and 16 m long (Fig. 2).

A 4H:1V (14°) slope was prepared to replicate a typical design for waste cover slope (Stark and Newman, 2010). The GMB installed had a typical 11 mm-diameter circular hole (Giroud and Bonaparte, 1989) in each section, positioned about 5 m down-slope from the crest. The three sections, each 4.9 m wide and extending 8.1 m along the 4H:1V slope, were excavated in silty sand, following the placement of GMB and a top layer of cover soil. Construction was conducted in February with temperatures below freezing, and there was ample local snow to facilitate construction of Section C as described below.

Sections A and B were previously described by Fan et al. (2024). The focus of this paper is on Section C, although comparisons will be made with the performance of Sections A and B (Figs. 2–4). All three sections were designed to be nominally identical except as detailed below.

(A) Reference Section A was built to evaluate leakage through a GMB hole on a 4H:1V slope without differential settlement.
(B) Section B was built with a dish-shaped depression (3 m wide, 2 m long, and 0.3 m deep), backfilled with a snow/sand (1:1 by volume) mixture to bring the slope back to a uniform 4H:1V slope (Fig. 4b). The GMB layer was placed over both the slope and snow/sand mixture. Post-snowmelt, a 0.15m depression developed below the GMB and was reflected on the surface as a dish-shaped trough (Fig. 4c) arising from the differential settlement due to the melting of the snow in the snow/sand mixture.
(C) Section C was built such that initially it had a dish-shaped depression identical in depth to that developed after snowmelt in Section B (3 m wide, 2 m long, and 0.15 m deep), with the GMB placed on the base of the slope and depression (Fig. 4b). Unlike Section B, Section C's cover soil surface was releveled, representing a waste cover that had been repaired by backfilling with the original soil material to re-establish the original slope following differential settlement.

In this study, the term "surface trough" specifically refers to the depression observed on the surface after snowmelt in Section B (Fig. 4c), differentiating it from the depression beneath the GMB layer. The design of the depression shape was informed by previous studies on differential settlement (Maurice, 2002; Scalia et al., 2017; Warith et al., 1994). A geotextile with an apparent opening size of 0.21 mm and high permeability was used above the GMB hole to prevent sand intrusion and clogging.

The cover soil, a poorly graded medium-to-fine sand (ASTM D2487, 2011), was analyzed by sieve analysis (ASTM D422-63, 2007). Under the same compaction condition as the field, laboratory measurements of porosity and saturated hydraulic conductivity of the cover soil were measured (ASTM D5084 - 16a, 2016) (Table 1).

Instead of the typical 1.5-mm or 2 mm-thick high density polyethylene (HDPE) GMB, a 0.15 mm vapour barrier was used because of its flexibility which allowed convenient placement following the contours of the depression in Section C under cold weather conditions. The thinner vapour barrier allowed minimizing construction wrinkles compared to the traditional HDPE GMB (Rowe and AbdelRazek, 2019; Touze-Foltz et al., 2021; Xie et al., 2023). The vapour barrier's strength and interface friction angle with sand were tested to ensure they met the experimental requirements before the field experiment (Fan et al., 2022).

2.2. Construction details

Similar to the construction of Sections A and B (Fan et al., 2024), Section C was constructed following the steps summarized below in February 2022.

- Clearing snow and excavating frozen soil to create a 4H:1V slope.
- Removing protrusions that could damage the GMB and smoothing the surface.
- Excavating a 3 m × 2 m × 0.15 m depression (Fig. 5).
- Installing plumbing for leakage collection, including connection pipes for transferring water from the GMB hole to the flow gauge in Section C.
- Placing a GMB layer with a hole above the slope, ensuring that any wrinkles and gaps in the interface were minimized.

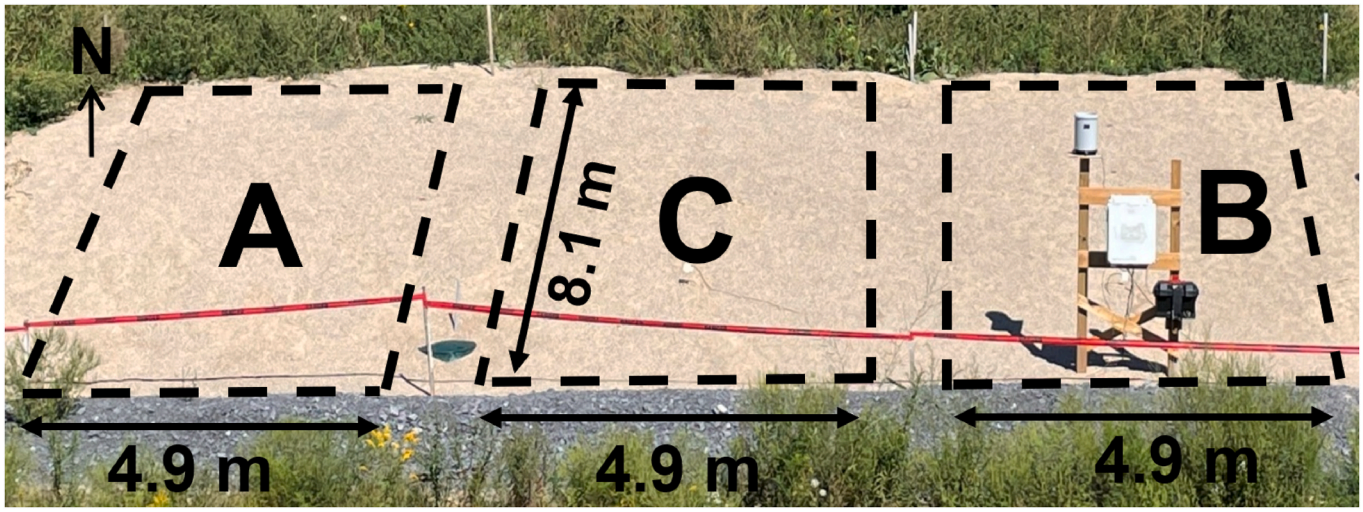

Fig. 2. Constructed sections A, B and C.

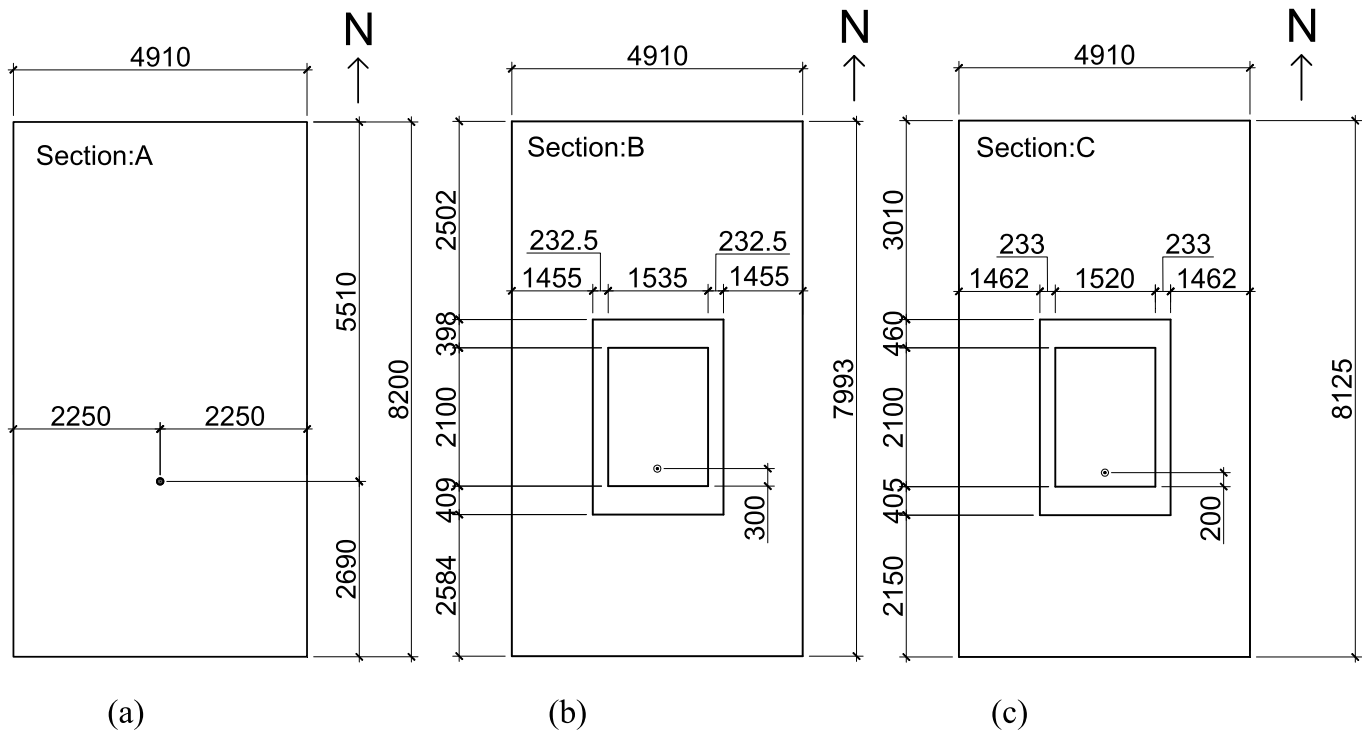

Fig. 3. Plan View schematic of Sections A, B and C.

- Placing a 0.3 m layer of cover soil (sand) over the GMB and installing the gravel pile at the foot of the sections for drainage and slope support.
- Shaping a 2-m-wide crest with a 3% slope to the north.
- Conducting an as-built survey during construction (Figs. 3 and 4).
- Installing instrumentation, including a rain gauge, three flow gauges, and four soil volumetric water content reflectometers, that were connected to a data acquisition system located at the toe of the slope on June 30, 2022.

2.3. Inspection

After the snowmelt in April 2022, Sections A and B were inspected and surveyed to confirm the location of the GMB holes. The depression depth (GMB layer) close to the hole in Section B was surveyed again in December 2022 and found to be between 0.12 m and 0.17 m while the maximum depth of the surface trough was surveyed to be 0.14 m (Fan et al., 2024).

During construction in February 2022, the GMB hole at Section C was placed 2 cm above the base of the depression due to the thickness of pipe connections(Fig. 6). The maximum depression depth was 0.45 m. The distance from the hole to the cover soil surface was 0.43 m. During each data collection visit, it was inspected and no vegetation was present on any of the leakage sections.

3. Experimental data and discussion

The continuous leakage data corresponding to the precipitation, calibrated volumetric water content, and temperature are shown in Fig. 7. For each period featuring rainfall events, the corresponding leakage data are detailed from Figs. 8–12 (the numerical results will be discussed later) and Tables 2 and 3. Fig. 13 and Table 4 display the monthly leakage data, corresponding to precipitation and the average soil temperature that was measured 15 cm above the hole in Sections B and C (Fig. 6a).

3.1. Observations: March 2022 to June 2022

Due to the availability issues of some instruments, the data were recorded during each field site visit (Table 2) at first. Leakage was collected and manually measured, rainfall was measured using a wireless rain gauge, and temperature was measured at the bottom of the snow/sand mixture and at the GMB layer using thermocouples. Supplementary rainfall and temperature data were obtained from a local weather station located in Hartington, approximately 16.1 km from QUELTS (Government of Canada, 2024).

No rainfall or leakage data was recorded during construction between mid-February and the end of February. From March to June 2022, there was no significant leakage in any sections except for period 12 (Table 2). One day before period 12 (period 11), it is likely that12 mm of rainfall was mostly stored in soil. On June 8, 2022 (period 12) there was an additional 25 mm of rainfall that resulted in 5.6 L of leakage in Section B but only 0.728 L in Section C. This difference can be attributed to the absence of a surface trough in Section C, which will be discussed later.

3.2. Observations: July 2022 to October 2022

On June 30, 2023, the instrumentation (a scientific rain gauge, tipping bucket flow gauges, and soil water content reflectometers) with dataloggers were installed to record data. This setup was tested and calibrated in a laboratory before installation. In Sections B and C, the volumetric water content was measured by water content reflectometers positioned 15 cm above the hole (Fig. 7).

The representative periods with leakage are shown in Table 3. Section C (surface repaired) consistently had lower leakage and lower VWC_0 than Section B (surface trough). In period 16 (July 12, 2022) and period 17 (July 18, 2022), the leakage measured in Section C was less than 5% of the leakage measured in Section B. This indicates that the precipitation (25.4 mm–29.6 mm) had just exceeded the threshold required to surpass the field capacity (the upper limit of volumetric water content of soil after excess water has drained) of cover soil in Section C and resulted in only a minor amount of leakage. The same amount of precipitation

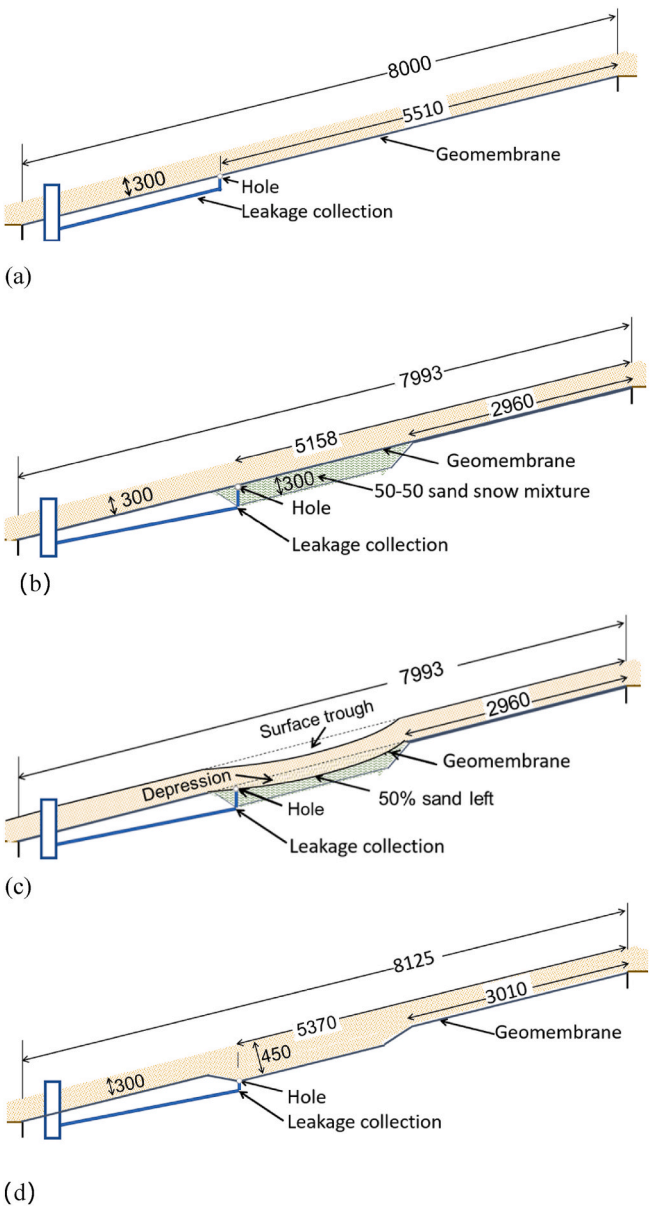

Fig. 4. Cross sections of the field GMB leakage experiments: (a) Section A; (b) Section B initial condition; (c) Section B after snowmelt; (d) Section C.

Table 1
Properties of Poorly graded medium-to-fine sand cover soil.

Property	Value
Measured:	
Porosity	27%
Saturated k_{global} (k_{ref}) (m/s) at 21.9 °C	2.2×10^{-4}
Dry density of soil (kN/m^3)	17.9
D_{10} (mm)	0.16
D_{60} (mm)	0.7
D_{85} (mm)	2
Unified Soil Classification	SP
Assumed:	
Maximum suction (kPa)	1000
Residual volumetric water content	5%
Compressibility (kPa)	0

resulted in 4.4 L–12.7 L more and earlier leakage in Section B than Section C. This implies that the additional soil used to backfill the surface trough increased the water storage capacity above the hole in Section C and raised the threshold compared to Section B (see arrow pointing to periods 16 and 17 in Fig. 7, showing the different *VWC* between Sections B and C). An additional 38 mm of rain in period 18 (July 24–25, 2022) pushed Section C to its field capacity and once this (higher) threshold was reached it also leaked in period 19 (45 mm on August 21, 2022). Leakage was observed at all three sections during period 20 (August 22-23, 2022), with even higher precipitation (114.6 mm) and the difference between Sections B and C narrowed compared to periods 16 and 17 (Table 3).

Observing the leakage in the three sections before and after the rainfall event in period 20, two different mechanisms affecting leakage for Section C can be identified. The first has already been discussed above and that is storage capacity, the backfilling of the surface settlement trough at Section C increases storage capacity, thereby increasing the threshold of water required to induce leakage and consequently reducing leakage significantly during rainfall events that did not reach that threshold. In short, the additional storage due to backfilling at Section C substantially reduces the number of rainfall events that can contribute to leakage relative to Section B. The second mechanism that becomes apparent is the size of the collection zone. At Section B, there are depressions both below the cover soil and above the cover soil, but at Section C, there is only a depression below the cover soil. At section A, there is no trough so the storage of section A is essentially the same as at Section B, thus the difference in leakage between Sections A and B may be attributed to a combination of effect of the trough above and below the cover soil. Once the threshold is reached, the difference between the leakage at Sections B and C can be largely attributed to the surface trough above the cover soil. Specifically, the leakage in period 20 suggests that, until a local flood (discussed below) interrupted measurement, approximately 5.3 L (27.7 L in Section B - 22.4 L in Section C) or 19% of leakage at Section B is due to the surface trough, and 12.7 L (22.4 L in Section C - 9.7 L in Section A) of leakage at Sections B and C (46% of leakage at B and 57% of leakage at C of the total leakage) was due to the depression below the cover soil, with the remaining 9.7 L (35% of leakage at B and 43% of leakage at C) being what would be expected to leak in the absence of differential settlement (Section A).

The rainfall events in period 20 (August 22 to 23, 2022), with a total of 114.6 mm of precipitation and a maximum precipitation rate of 38 mm/h gave rise to a local flood with the water level in the sumps causing the tipping bucket flow gauges to become submerged beneath the water table and consequently interrupting data collection until the water table receded (Fig. 10). The gauges became functional again once the flood subsided.

3.3. Observations: November 2022 to February 2023

From period 22 to 28 (November 30, 2022, to February 15, 2023), leakage collected in Section C was consistently lower, ranging from 0.5% to 66% of leakage in Section B (Table 3). The maximum leakage occurred in Section B (99.8 L) in period 24 (from December 30, 2022, to January 1, 2023), while the leakage measured in Section C was only 28.9 L.

Although there was less measured precipitation from November 2022 to February 2023 (a total of 284.4 mm) than from July to October 2022 (a total of 448.4 mm) (Table 4), the total leakage of both Section B and Section C from November 2022 to February 2023 (Sec. B of 281.3 L vs Sec. C of 114.6 L) was larger than that from July 2022 to October 2022 (Sec. B of 136.1 L vs Sec. C of 76.8 L) (Table 4, Fig. 13). This can be explained by the lower hydraulic conductivity and less evaporation in colder temperatures (Fan et al., 2024.). Similar observations have been reported by Wilson et al. (1993) and Weeks and Wilson (2005).

The soil temperatures measured in both sections were consistently above 0 °C, even with the lowest daily average air temperature of −23.3 °C (February 3, 2023, in Fig. 7). The observation of persistent soil temperature above 0 °C is consistent with other measurements at QUELTS where the temperature of the geomembrane in winter rarely

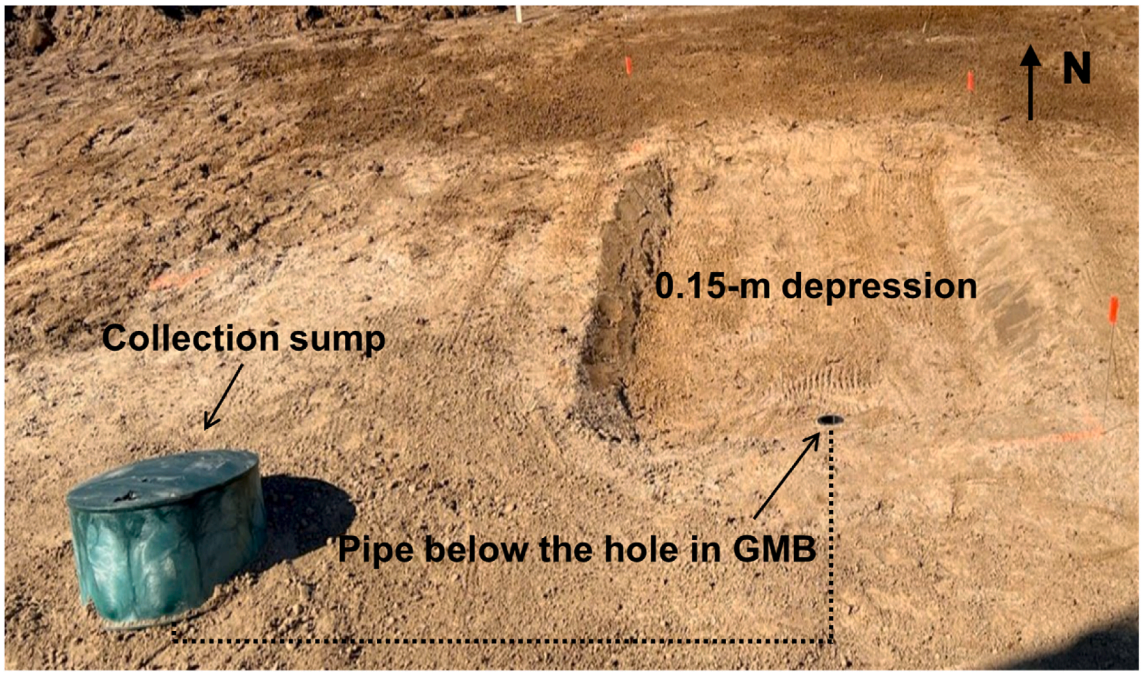

Fig. 5. Section C prior to placement of GMB and cover soil.

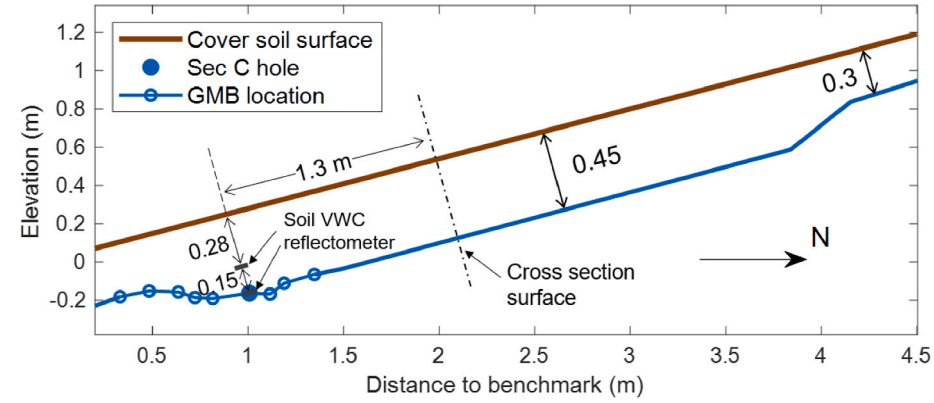

(a) Sec C south-to-north direction

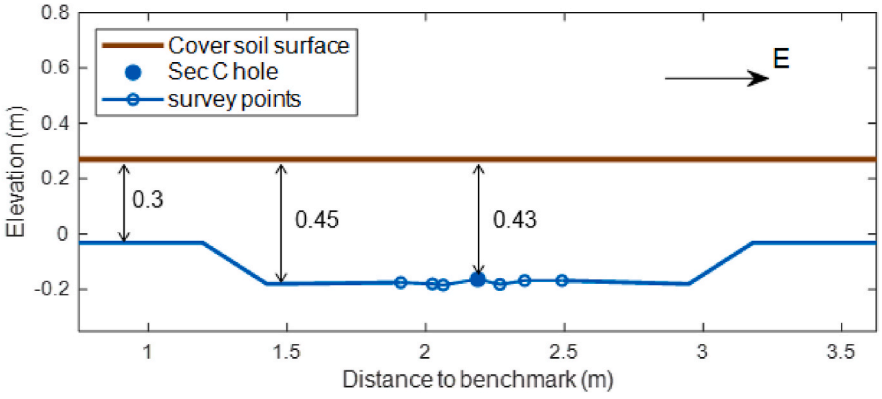

(b) Sec C west-to-east direction

Fig. 6. Survey data points for Section C in cross-section view at the intersection with the hole.

went below 0 °C with cover soil or snow over the geomembrane (Take et al., 2015). The soil temperature was consistently above 0 °C in both sections because snow and sand are good insulators to maintain the temperature. As a result, the water could flow through the cover sand and cause leakage even at an extreme low air temperature. The effectiveness of this mechanism at QUELTS with 0.3 m of cover soil could be sustained for about 2 months consistently below −20 °C. In other locations where either the temperature is substantially lower than −20 °C

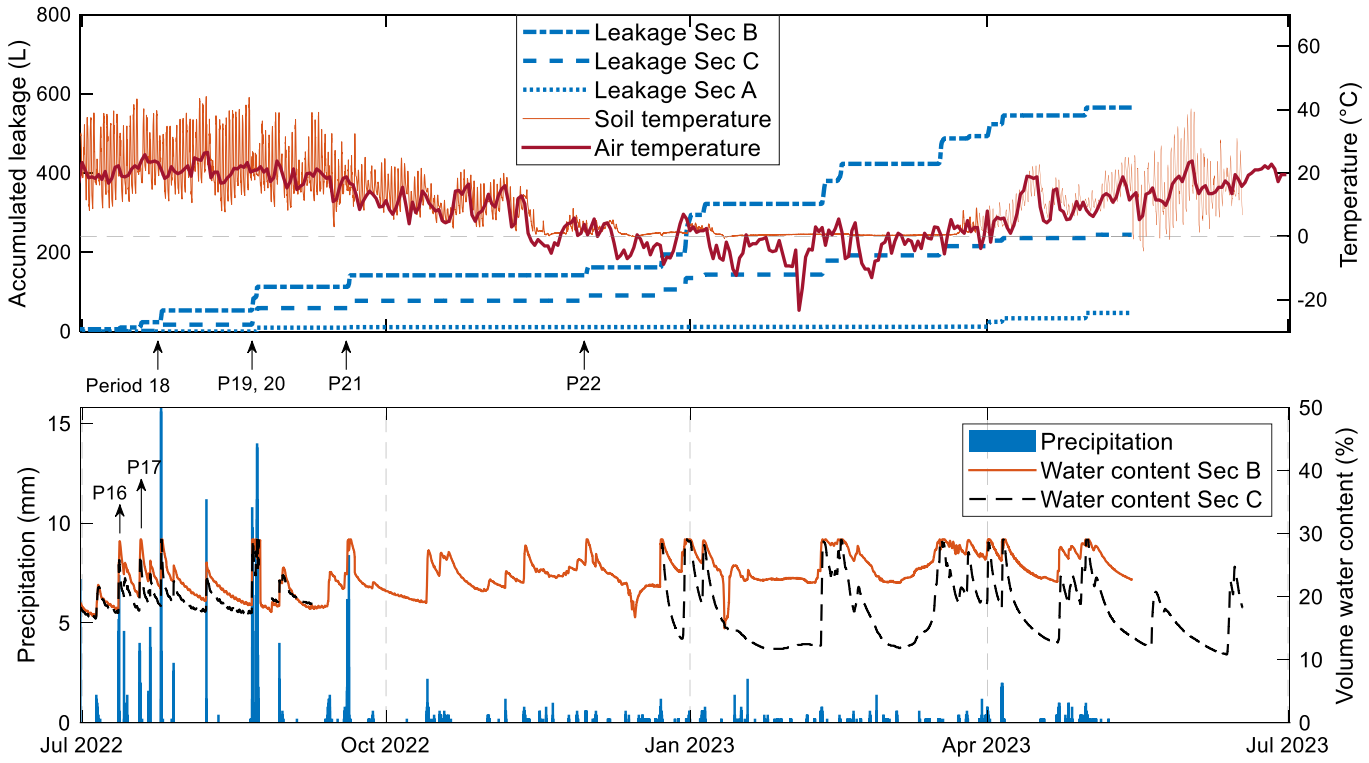

Fig. 7. Instrumentation measurements of precipitation, leakage, and volumetric water content from July 2022 to April 2023.

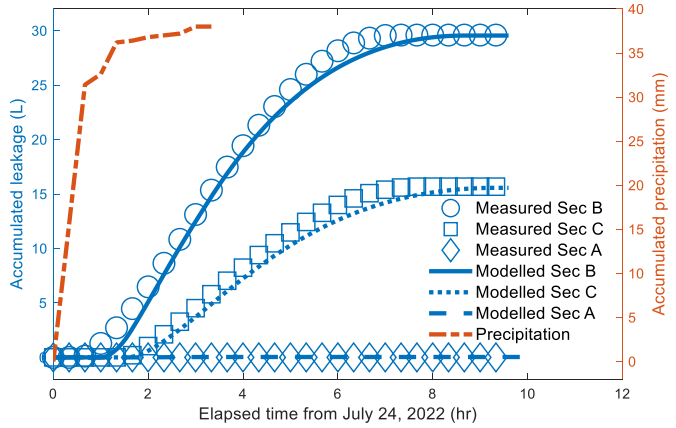

Fig. 8. Leakage over time following 38 mm rainfall event since July 24 (Period 18).

or it is sustained at −20 °C for a substantially longer time, freezing can be expected to migrate deeper and eventually stop the flow.

3.4. Discussion of observations

3.4.1. Effect of precipitation on VWC and leakage

Before December 2022, the precipitation (rainfall) always resulted in the increase of volumetric water content but did not necessarily trigger leakage (Fig. 7). This is because the leakage would not occur until the amount of precipitation surpasses the threshold to raise the volumetric water content (*VWC*) of the sand close to the hole to the field capacity (close to the soil porosity of 27% in Fig. 7). For example, on October 13, 2022, the precipitation raised the *VWC* by around 7% in Section B without inducing any leakage because the post-rainfall *VWC* was below field capacity. The initial water content (VWC_0) before rainfall is also a significant factor that influenced leakage. For example, in time period 21 (September 19 to 20, 2022), although the precipitation (24.6 mm) was close to that of period 16 (25.4 mm on July 12, 2022), the leakage in Sections B and C in period 21 was much larger because the measured VWC_0 in period 21 is 10.6% higher than period 16 based on Section B measurement (Table 3). This demonstrates the importance of considering VWC_0 when predicting leakage behaviour.

Since December 2022, not all the precipitation increased the *VWC* (Fig. 7), this is because the snowfall could accumulate on the surface of the cover without melting during periods of below-freezing temperatures. Winter inspections revealed that the snowpack above the cover mirrored the surface trough shape in Section B when snow was absent, indicating the difference of snow thickness above the surface trough is negligible compared to other areas in the section. The snowpack would eventually melt and increase the *VWC* in the cover soil as the temperature increased above 0 °C. For instance, despite no precipitation (February 14 to 15 in Period 27 in Table 3), the air temperature rose up to 12 °C and led to snowmelt from previous snow accumulations. This resulted in leakage in both Sections B and C.

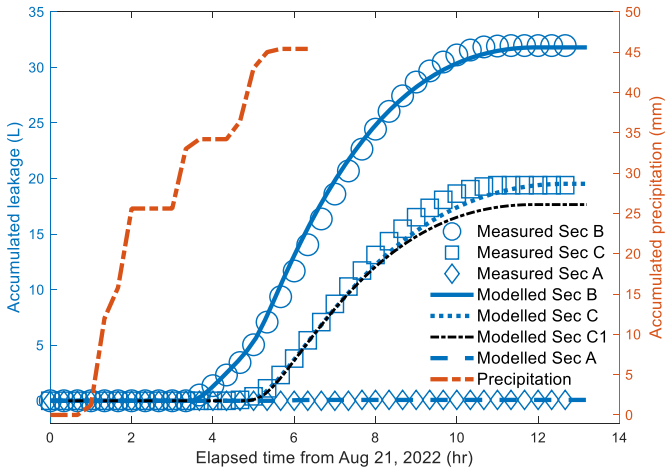

Fig. 9. Leakage over time following 45 mm rainfall event since August 21 (Period 19).

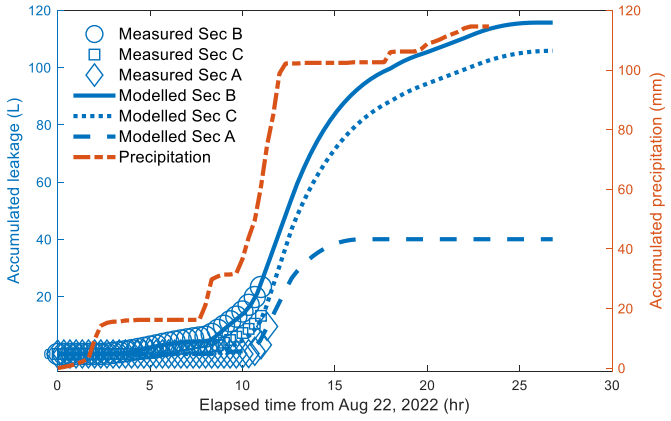

Fig. 10. Leakage over time following 114.6 mm rainfall event since August 22 (Period 20) [monitoring equipment malfunction after 10 h due to a local flood].

3.4.2. Seasonal effect on leakage difference between sections B and C

The difference in the leakage between Sections B and C (Table 4, Fig. 13) is seasonal. Given an equivalent time of five months, the total leakage in Section C (77.6 L) was 55% of that in Section B (141.8 L) from June to October 2022 (average soil temperature of 19 °C), but this ratio dropped to 39% (351.3 L in Section B vs 137.8 L in Section C) from November 2022 to March 2023 (average soil temperature of 2 °C). This indicates that filling the surface trough was effective in reducing the leakage in both seasons, and particularly effective during cold temperatures in the experiment. The results suggest that the benefits of filling the surface trough are not limited to warm regions but are also effective in cold regions experiencing extended periods of below-freezing temperatures.

4. Summary

Over the 15-month period and a total precipitation of 1260 mm, the total leakage in Section C was 244 L, which is 43% of that in Section B (565 L), demonstrating that filling a surface trough (roughly 3 m × 2 m x 0.14 m) can substantially reduce the leakage. Additionally, increased leakage through a hole typically has a higher risk of washing out fine particles from the subgrade and causing higher levels of local settlement. Therefore, once a surface trough reaches certain thresholds (e.g., 3 m × 2 m × 0.14 m in this study), it is recommended to undertake remediation to manage surface settlements, such as backfilling the surface trough.

5. Numerical modelling

Transient finite element seepage analyses of the three sections were conducted using the SEEP 3D program (GeoStudio, 2021) for several percolation events. Alternative software such as HYDRUS (Benson et al., 2007; Breitmeyer et al., 2019) could also have been used. Each package has strengths and weaknesses. The GeoStudio software was selected here because it is widely used by consultants due to its broad range of geotechnical engineering capabilities (e.g., integration with SLOPE/W and CTRANS) which facilitates potential future slope stability analyses. Also, SEEP 3D had been validated using previous experimental data from Sections A and B (Fan et al., 2024). This paper will continue to use the validated 3D model and primarily focus on the comparison between Section B and Section C. The numerical analysis aims to help understand the differences between the two sections and investigate additional factors affecting leakage.

5.1. Assumptions

To optimize the numerical modelling process and improve efficiency, the modelling was conducted subject to the following assumptions.

- The cover soil (sand) is isotropic and homogeneous, except where otherwise noted, with the properties given in Table 1. The sand experienced no reduction in volume (zero compressibility) for the modelled leakage events since July 2022, 4 months after construction.

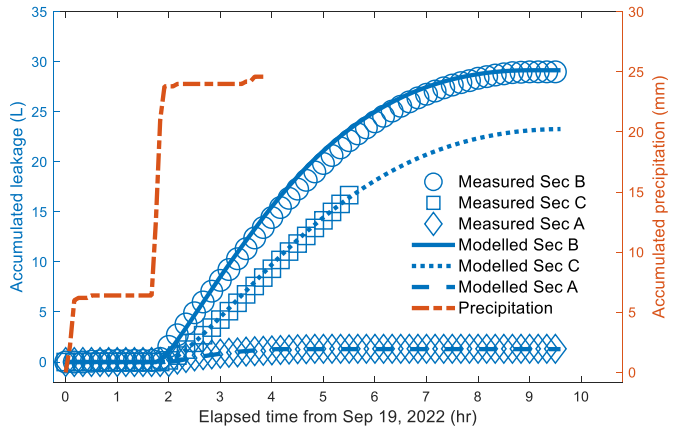

Fig. 11. Leakage over time following 24.6 mm rainfall event since September 19 (Period 21).

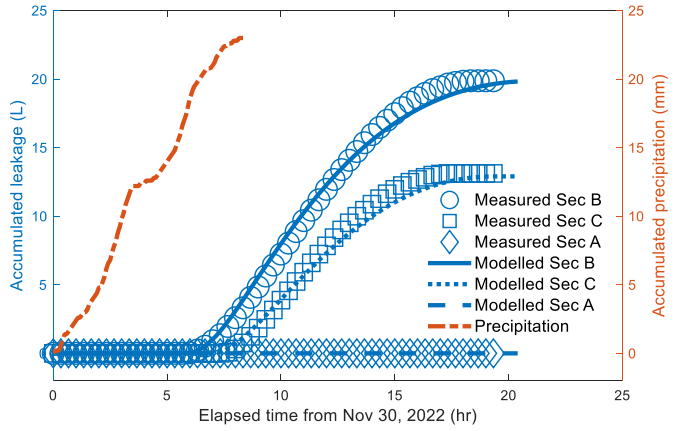

Fig. 12. Leakage over time following 23.1 mm rainfall event since November 30 (Period 22).

- The initial water content (VWC_0) of cover soil before the modelling of each rainfall event is spatially homogeneous (Table 5).
- The soil temperature is the average reading recorded during the modelled event.
- The cover soil within five-hole diameters from the hole had experienced a washout of fine particles (Fan et al., 2024; Rowe and Fan, 2021), giving rise to an increased local hydraulic conductivity (k_{local} as discussed later).
- The geometry of the depression and the location of the hole in Section C are based on the corresponding survey data (Fig. 6).
- Precipitation is consistent across all three sections, showing no spatial variation.
- There are no wrinkles in the GMB in the sections analyzed.
- Leakage is defined as the fluid entering the hole.

5.2. Model details

5.2.1. Model parameters

The saturated hydraulic conductivity (k) modelled for different rain events was calculated as a function of the viscosity of water related to temperature (Hopmans and Dane, 1986):

$$k_T \Big/ k_{ref} = \mu_{ref} \Big/ \mu_T \tag{1}$$

where k_{ref} and k_T are the saturated hydraulic conductivity of the cover soil at the reference temperature in the laboratory (21.9 °C) and measured soil temperature in the field, respectively. μ_{ref} and μ_T are the viscosity of water at the reference temperature (21.9 °C) and measured soil temperature respectively, using the empirical relationships provided in the CRC Handbook of Chemistry and Physics (Lide, 2005). The different saturated k values for different cover soil temperatures monitored during each modelled rainfall event were used accordingly (Table 5).

Within the material definition interface in the software, the volumetric water content function (VWC vs suction) was derived based on the built-in standard sample function for sand and its particle size distribution (Aubertin et al., 2003). The hydraulic conductivity (k) function (unsaturated k vs suction) of the cover soil was obtained using the built-in Van Genuchten model (Van Genuchten, 1980), in conjunction with the volumetric water content function. The relevant soil parameters input are listed in Table 1. More details about the cover soil are elaborated in Fan et al. (2024), where the same sand was used.

Rowe and Fan (2021) showed that a 3% reduction in fine content around a hole in the liner could double leakage. Consequently, the soil samples from the field, where particles finer than 0.2 mm had been washed out (a geotextile with an apparent opening size of 0.21 mm was placed above the hole), were tested in the laboratory. These tests showed that the saturated $k_{local} = 1.4 \times 10^{-3}$ m/s. This indicates that k_{global} (k_{ref}) $= 2.2 \times 10^{-4}$ m/s could increase to $k_{local} = 1.4 \times 10^{-3}$ m/s for the local soil within five diameters of the hole at 21.9 °C if the fine particles (<0.2 mm) are all washed out (Fan et al., 2024). The k_{local} (k_{ref}) values started same as k_{global} (k_{ref}) and increased over time with more leakage washout (Table 5). Thus, Section B with the larger flow (leakage) and consequent earlier washout of mobile fines exhibited higher k_{local} (k_{ref}) compared to Section C during periods 18 to 20. However, the saturated k_{local} (k_{ref}) across all three sections stabilized at 1.1×10^{-4} m/s in periods 21 and 22 (Table 5), likely due to the mobile fines having been lost and the rest having established a stable structure.

Table 2
Manually monitored leakage and climate data: February to June 2022.

Period	Date range (y-m-d)	Rainfall [a] (mm)	Leakage (L)			Temperature [b] (°C)		
			Sec. A	Sec. B	Sec. C	Air	Base of mixture	GMB
1	22 Feb 15 - Feb 18	NA	0	NA [c]		−10.1	0.6	0.9
2	22 Feb 18 - Feb24	NA	0			−2	1.5	0.8
3	22 Mar 5 - Mar 18	20.5	0	0.025	0.075	1.1	NA	NA
4	22 Mar 18 - Mar 24	18.6	0	0	0	5.5	4.7	4.6
5	22 Mar 24 - Apr 5	NA	0	0.014	0.037	13.3	NA	6.3
6	22 Apr 6 - Apr 08	24	0	0.03	<0.001	11.7	NA	7.1
7	22 Apr 8 - Apr16	7.7	<0.001	<0.001	<0.001	9.3	7.1	9.1
8	22 Apr 16 - Apr 22	40	0	0	0	16.9	6.3	9
9	22 Apr 22 - May 5	36	0	0	0	22.7	9.7	11.8
10	22 May 5 - June 3	91	0	0.125	0.059	21.9	16.6	17.4
11	22 Jun 6 - Jun 7	12	0	0	0	19.5	NA	NA
12	22 Jun 7 - Jun 8	25	0	5.6	0.728	25.3	NA	NA
13	22 Jun 8 - Jun10	6	0	0.001	0.002	18.2	16.7	17.1
14	22 Jun 10 - Jun 23	1.1	0	0	0	20	NA	NA
15	22 Jun 23 - Jun 30	7.2	0	0	0	22	NA	NA

[a] The rainfall was measured using an on-site wireless electronic rain gauge.
[b] The average air temperature for each period was sourced from the local weather station (located in Hartington, approximately 16.1 km from QUELTS). The temperatures were measured upon each visit, using a thermocouple located at the base of the sand/snow mixture in Section B and a thermocouple directly beneath the GMB of Section B.
[c] Sections B and C was being constructed during this period, so no data was collected.

Table 3
Instrument-monitored experimental data, July 2022 to May 2023.

Period	Date range (y-m-d)	VWC_0 [a]		Precipitation [b] (mm)	Section leakage (L)			Temperature [c] (°C)			
		Sec. B	Sec. C		A	B	C	Air maximum	Air minimum	Sec. B	Sec. C
16	22 Jul 12	18.0%	17.3%	25.4	0	4.4	0.04	26	18.5	23	20.9
17	22 Jul 18	20.0%	17.7%	29.6	0	13.3	0.6	23	20	21.4	21.7
18	22 Jul 24–25	21.2%	18.4%	38	0	29.6	15.7	26.5	18.5	20.8	20.8
19	22 Aug 21	18.6%	17.4%	45	0	32	19.4	23.5	17	22.7	22.7
20	22 Aug 22–23	27.4%	23.3%	114.6	9.7	27.7	22.4	23	19	22.1	22.1
21	22 Sep 19–20	28.6%	NA	24.6	1.3	29	18.5	22.5	15	15.1	NA
22	22 Nov 30 - Dec 1	25.0%		23.1	0.08	19.9	13.1	7.5	−2	1.0	1.0
23	22 Dec 22–23	19.6%		44	0	32.6	15.1	3	−8.5	0.6	2
24	22 Dec 30–23 Jan 1	28.3%	22.5%	21.4	0.4	99.8	28.9	9	1	2.2	2.5
25	23 Jan 4–5	25.3%	19.0%	22.2	0.08	27.7	8.5	3.5	0	2.1	3
26	23 Feb 9–11	24.0%	12.2%	27.8	0.04	58	35.2	6.5	−6	0.6	1.3
27	23 Feb 14–15	29.0%	25.2%	0	0	8.24	0.04	12	−2	0.8	1.3
28	23 Feb 15	29.0%	26.3%	1	0	34.8	13.2	12	−1	0.7	1.2
29	23 Mar 17–18	28.6%	25.5%	8.6	0.36	64	23.2	5	−2.5	0.5	1
30	23 Mar 26	26.8%	20.1%	14.4	0	5.8	0	9	1	2.8	2.5
31	23 Mar 31- Apr 1	26.0%	18.8%	27	0	30.1	13.9	16.5	−4	3.2	2.9
32	23-Apr-05	25.7%	18.3%	40.6	5.2	22	6.4	12	−1	3.8	5.3
33	23-Apr-30	28.4%	24.9%	29.2	0	19.8	8.2	12.5	9	10.7	10.5

[a] The initial volumetric water content (VWC_0) was measured 15 cm above the hole (see Fig. 6). The VWC_0 measurements are accurate to within ±3%, reflecting the range of potential deviation from the true value.
[b] Precipitation, including both rain and snow, was measured using a scientific rain gauge since June 30, 2022.
[c] The maximum and minimum air temperatures were obtained from the same local weather station. The average soil temperature was calculated based on the measurements by soil water content reflectometers installed in July 2022.

Because k values decrease when the soil is not fully saturated, the volumetric water content function and the hydraulic conductivity function of the soil are defined based on validated settings for the same soil material at this site (Fan et al., 2024). The soil property inputs needed for the program (e.g., maximum suction and residual volumetric water content) are shown in Table 1.

5.2.2. Boundary conditions

The boundary conditions are illustrated in Fig. 14. Each of the three sections was subjected to identical precipitation boundary conditions. Due to the inability of the 3D version of the program to calculate surface runoff directly, the measured precipitation was initially applied to the slope surface within the 2D model to calculate surface runoff so that the net infiltration can be applied in the 3D models (Fan et al., 2024). However, the 2D model results showed no surface runoff for any of the rain events at QUELTS. For the hole and the downslope area of the cover sand, the boundary conditions were achieved by activating the 'Potential Seepage Face Review' option in the 3D program. This feature allows the software to dynamically identify where seepage (outflow) might occur on the modelled surface.

5.3. Modelling results and discussion

The numerical analysis covered five representative events (periods) featuring rain events from July to November 2022 (Table 5). Since the software lacks the capability to simulate the coupled effect of infiltration from snowfall, snowmelt, and rainfall, scenarios involving snow precipitation are beyond the scope of this paper.

5.3.1. Numerical results vs experimental data

The results of numerical analyses are in good agreement with observed leakage during rainfall events for all three sections,

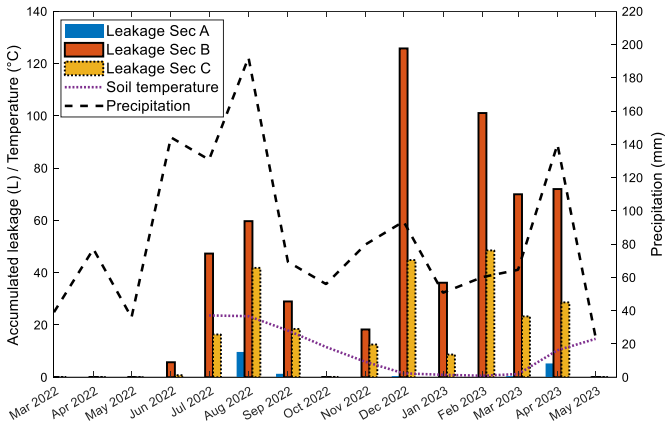

Fig. 13. Monthly precipitation, soil temperature and leakage measurements.

Table 4
Monthly leakage summary over a 15-month period.

Year-Month	Monthly Section leakage (L)			Precipitation [a] (mm)			Temperature [b] (°C)	
	A	B	C	On-site Measured	Local Weather Station		Average Air	Average Soil
					Rain	Snow		
22 Mar	0	0.025	0.075	39.1	41.6	26	−1.5	NA
22 Apr	<0.001	0.045	0.039	77.1	71.2	11	6.8	
22 May	0	0	0	36	94.4	0	15.3	
22 Jun	0	5.74	0.79	144.2	95	0	17.6	
22 Jul	0	47.32	16.36	130.8	132.6	0	20.8	23.6
22 Aug	9.68	59.72	41.84	192.2	120.2	0	21.1	23.4
22 Sep	1.32	29.00	18.48	69.4	45.6	0	15.7	17.9
22 Oct	0	0.04	0.12	56	57.8	0	9.7	11.6
22 Nov	0.08	18.28	12.52	79.8	73.8	8	4.4	5.9
22 Dec	0.44	125.80	44.84	93.6	68.2	48	−1.5	1.5
23 Jan	0.08	36.16	8.68	50.8	28	48	−3.4	0.9
23 Feb	0.08	101.08	48.52	60.2	36	26	−4.4	0.6
23 Mar	0.44	70.00	23.28	64.6	51	34	−0.3	1.2
23 Apr	5.28	72	28.64	140	127.6	0	8.8	10.3
23 May [b]	0.08	0.04	0.04	24	17	0	12.7	14.7
Sum	17.5	565.3	244.2	1257.8	1060.0	152	–	–

9 Data for May 2023 is from May 1st to May 14th only.
[a] The rain and snow precipitation from the local weather station are provided respectively for comparison.
[b] Average air and soil temperatures were obtained from the local weather station and measurements from soil water content reflectometers, respectively. Data before July is unavailable to limited access to soil reflectometers.

corresponding to the 38 mm rainfall in time period 18 (July 24 to 25, 2022) in Figs. 8 and 45 mm in time period 19 (August 21, 2022) in Figs. 9 and 114.6 mm in time period 20 (August 22 to 23, 2022) in Figs. 10 and 24.6 mm in time period 21 (September 19 to 20, 2022) in Figs. 11, and 23.1 mm in time period 22 (November 30 to December 1, 2022) in Fig. 12. The numerical results successfully replicate the observed pattern of leakage, which consistently occurred in the sequence of Sections B, C, and A. The slight discrepancies between the modelling results and experimental data can be attributed to the assumptions outlined in Section 4.1, along with the inherent limitations in the precision and accuracy of the field construction, instrumentation, and survey measurements.

5.3.2. *Effect of discrepancies in geometries*

Although experimental data revealed a substantial (~2-fold) difference in leakage between Section B and Section C, this difference cannot be entirely attributed to the surface trough, given the discrepancies in geometries and hole locations between the two sections due to construction limitations. For example, Fig. 3 shows that the distance between the hole and the depression lower bound is different (300 mm in Section B vs 200 mm in Section C). Consequently, an idealized Section C_1 (Table 5), mirroring Section B's geometries but without the surface trough, was compared with Section C for period 19 to assess the sensitivity of leakage data to these geometric differences. The numerical results between Section C_1 (Fig. 9) and Section C indicate that geometrical variations account for only about 10% of the difference in leakage and infer that the effect of the surface trough is likely about 10% greater than implied by the experimental data.

5.3.3. *How surface trough and depression affect leakage*

The accumulated downslope water flux in period 19 was numerically simulated (Fig. 15) with attention focused on the nodes at the bottom of the cross-section surface located 1.3 m upslope from the hole (dot-dashed line in Fig. 6a). In both Sections B and C, higher water flux is observed through the depression area ($-1 < x < 1$ m). Quantitatively, in both Sections B and C, the numerical output showed around 45% of the total flux was concentrated through the depression area, with an identical catchment width of approximately 2.25 m (45% of the total 5 m). This width exceeds the physical depression width of about 2 m (dashed line in Fig. 15), indicating that infiltration from outside the depression width is channeled into it, drawn by the lower water pressure head.

Sections B and C displayed identical catchment widths (2.25 m). However, Section C consistently shows less water flux across the entire 5-m section width due to its lower initial volumetric water content (VWC_0) (Fig. 7). Therefore, Section C, compared to Section B, experiences less leakage due to the additional soil above the hole, which leads

Table 5
Numerical modelling parameters and results.

Period	Date (2022)	Section	Modelled VWC_0	Soil temperature (°C)	Viscosity [a] (mPa·s)	k_{global} [b] k_T (m/s)	k_{local} k_{ref} (m/s)	k_{local} [b] k_T (m/s)	*Leakage Q (L)*
Lab test	–	–	–	21.9	0.954	2.2×10^{-4}	2.2×10^{-4} -1.4×10^{-3}	–	–
18	Jul 24	A	10.0%	20.8	0.982	2.2×10^{-4}	2.2×10^{-4}	2.2×10^{-4}	0
	–	B	11.3%				9.7×10^{-4}	9.5×10^{-4}	29.6
	Jul 25	C	10.0%				7.7×10^{-4}	7.5×10^{-4}	15.6
19	Aug 21	A	7.4%	22.7	0.939	2.2×10^{-4}	2.2×10^{-4}	2.2×10^{-4}	0
		B	9.6%				9.8×10^{-4}	1.0×10^{-3}	31.8
		C	8.1%				8.8×10^{-4}	9.0×10^{-4}	19.5
		C_1	8.1%				8.8×10^{-4}	9.0×10^{-4}	17.7
20	Aug 22	A	12.4%	22.1	0.952	2.2×10^{-4}	8.8×10^{-4}	9.0×10^{-4}	38.5
	–	B	13.9%				9.9×10^{-4}	1.0×10^{-3}	115.7
	Aug 23	C	12.0%				8.9×10^{-4}	9.0×10^{-4}	105.9
21	Sep 19	A	14.9%	15.1	1.135	1.9×10^{-4}	1.0×10^{-3}	8.5×10^{-4}	1.2
	–	B	15.6%				1.0×10^{-3}	8.5×10^{-4}	29.2
	Sep 20	C	14.8%				1.0×10^{-3}	8.5×10^{-4}	23.3
22	Nov 30	A	12.4%	1.0	1.731	1.2×10^{-4}	1.1×10^{-3}	6.0×10^{-4}	0
	–	B	13.1%				1.1×10^{-3}	6.0×10^{-4}	19.8
	Dec 1	C	13.1%				1.1×10^{-3}	6.0×10^{-4}	12.9

[a] The viscosity was derived from the measured soil temperature using the empirical equation (Lide, 2005).
[b] The k_{global} and k_{local} at field temperature (k_T) for saturated soil were calculated using equation (1) with $k_{ref} = 2.2 \times 10^{-4}$ m/s obtained from a laboratory test at 21.9 °C. k_{global} was utilized for modeling the hydraulic conductivity of the cover soil, except within a region spanning five diameters from the hole. Conversely, k_{local} was used specifically within this five-diameter region from the hole.

to a lower VWC_0 after each rain event. Section A, as the base case, showed a relatively stable water flux across the slope, indicating the catchment width around the hole is roughly equivalent to the hole diameter (11 mm), which accounts for the minimal leakage recorded in Section A.

5.4. Parametric study

Parametric studies were conducted using the model parameters from Sections B and C in period 19 (45 mm precipitation on August 21, 2022) as a base set of parameters (Table 5). Variations from this base set were analyzed to assess the impact of various factors and to enhance understanding in these key areas: i) hydraulic conductivity, ii) depression depth, iii) hole and depression location, and iv) slope gradient (Table 6).

5.4.1. Hydraulic conductivity (k_{global})

Three cover soil hydraulic conductivity (k_{global}) values for the sand cover soil were examined: (i) k_{global} @ 21.9°C–2.2×10^{-4} m/s measured for the sand used in the field, and two k_{global} values derived using Hazen's equation, k (m/s) = $0.01 \cdot (d_{10})^2$ (Hazen, 1893), for two representative d_{10} (in mm) values, where d_{10} is the particle diameter below

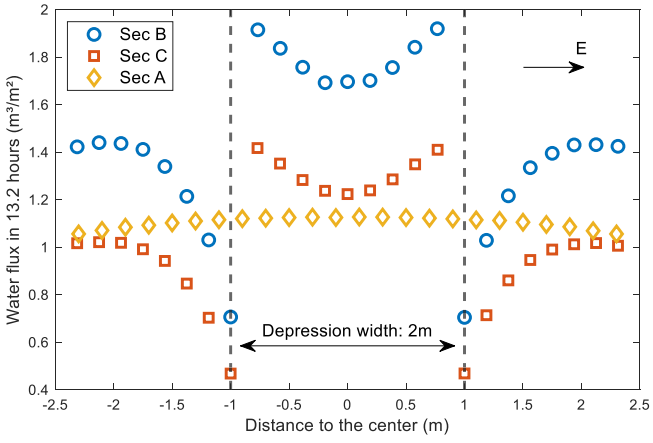

Fig. 15. Water flux distribution across the slope (west-to-east direction).

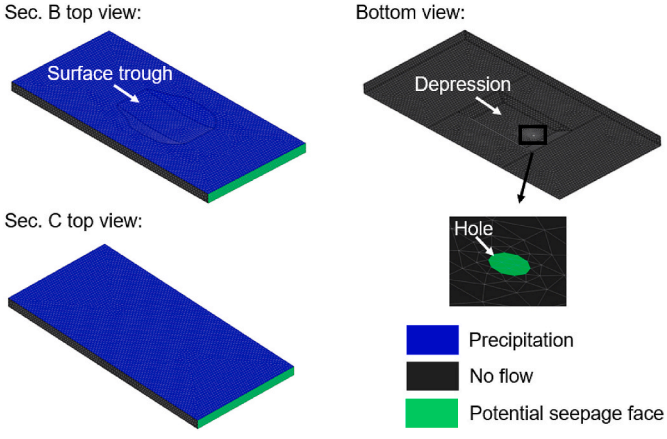

Fig. 14. 3D numerical model configuration and boundary conditions.

Table 6
Summary of parametric model results.

Case	k_{global}	Settlement depth	Upgradient slope length	Slope gradient	Hole Location	Leakage B	Leakage C
	(m/s)	(mm)	(m)	(°)		(L)	(L)
1	1.0 x 10^{-3}	150	3	14	Base	2.1	0.5
2	1.0 x 10^{-3}	300	3	14	Base	35.9	27.6
3	1.0 x 10^{-3}	450	3	14	Base	154	141.6
4	2.2 x 10^{-4}	150	3	14	Base	31.8	19.5
5	2.2 x 10^{-4}	300	3	14	Base	108.9	87.7
6	2.2 x 10^{-4}	450	3	14	Base	336	309.4
7	2.5 x 10^{-5}	150	3	14	Base	100.6	63.4
8	2.5 x 10^{-5}	300	3	14	Base	293.9	232.5
9	2.5 x 10^{-5}	450	3	14	Base	580	484.6
10	1.0 x 10^{-5}	150	3	14	Base	129.5	72.6
11	1.0 x 10^{-5}	300	3	14	Base	340.7	266.1
12	1.0 x 10^{-5}	450	3	14	Base	630	518.6
13	2.5 x 10^{-6}	150	3	14	Base	79	27.4
14	2.5 x 10^{-6}	300	3	14	Base	282.7	197.5
15	2.5 x 10^{-6}	450	3	14	Base	562	412
16	1.0 x 10^{-6}	150	3	14	Base	0	0
17	1.0 x 10^{-6}	300	3	14	Base	60	0
18	1.0 x 10^{-6}	450	3	14	Base	281	166.3
19	1.0 x 10^{-3}	150	7.4	14	Base	14.6	6.9
20	2.2 x 10^{-4}	150	7.4	14	Base	70.7	39
21	2.5 x 10^{-5}	150	7.4	14	Base	192.2	147.5
22	1.0 x 10^{-5}	150	7.4	14	Base	228.4	162
23	1.0 x 10^{-3}	150	11.8	14	Base	23.2	13.1
24	2.2 x 10^{-4}	150	11.8	14	Base	102.4	61.5
25	2.5 x 10^{-5}	150	11.8	14	Base	274.7	217.1
26	1.0 x 10^{-5}	150	11.8	14	Base	354	260
27	1.0 x 10^{-3}	150	3	14	Bottom	11	8.4
28	2.2 x 10^{-4}	150	3	14	Bottom	47.1	38.6
29	2.5 x 10^{-5}	150	3	14	Bottom	156	113.5
30	1.0 x 10^{-3}	150	3	5	Base	–	48.4
31	2.2 x 10^{-4}	150	3	5	Base	–	160.7
32	2.5 x 10^{-5}	150	3	5	Base	–	358
33	1.0 x 10^{-3}	150	3	2.9	Base	–	578.9
34	2.2 x 10^{-4}	150	3	2.9	Base	–	783.4
35	2.5 x 10^{-5}	150	3	2.9	Base	–	889.7

which 10% of the mass is finer, namely: (ii) $d_{10} = 0.05$ mm giving $k_{global} = 2.5 \times 10^{-5}$ m/s and (iii) $d_{10} = 0.32$ mm giving 1×10^{-3} m/s.

The lowest k_{global} (2.5×10^{-5} m/s) gave the largest leakage (63.4 L; Fig. 16) and this is consistent with the finding that lower k due to lower sand temperatures resulted in higher leakage (Fan et al., 2024). The right y-axis in Fig. 16 shows the water pressure head (above the hole) and the brown curves indicate the duration during which leakage occurred. Despite a lower peak water pressure head for $k = 2.5 \times 10^{-5}$ m/s compared to $k = 2.2 \times 10^{-4}$ m/s, the duration of positive water pressure is much longer (72 h for $k = 2.5 \times 10^{-5}$ m/s vs 13 h for $k = 2.2$

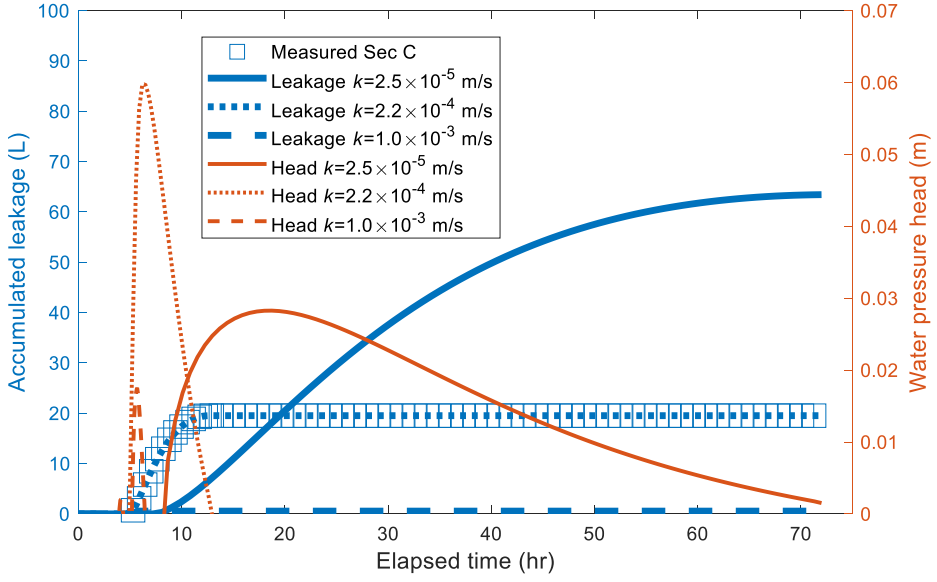

Fig. 16. Effect of hydraulic conductivity (k_{global}) on leakage and water pressure head.

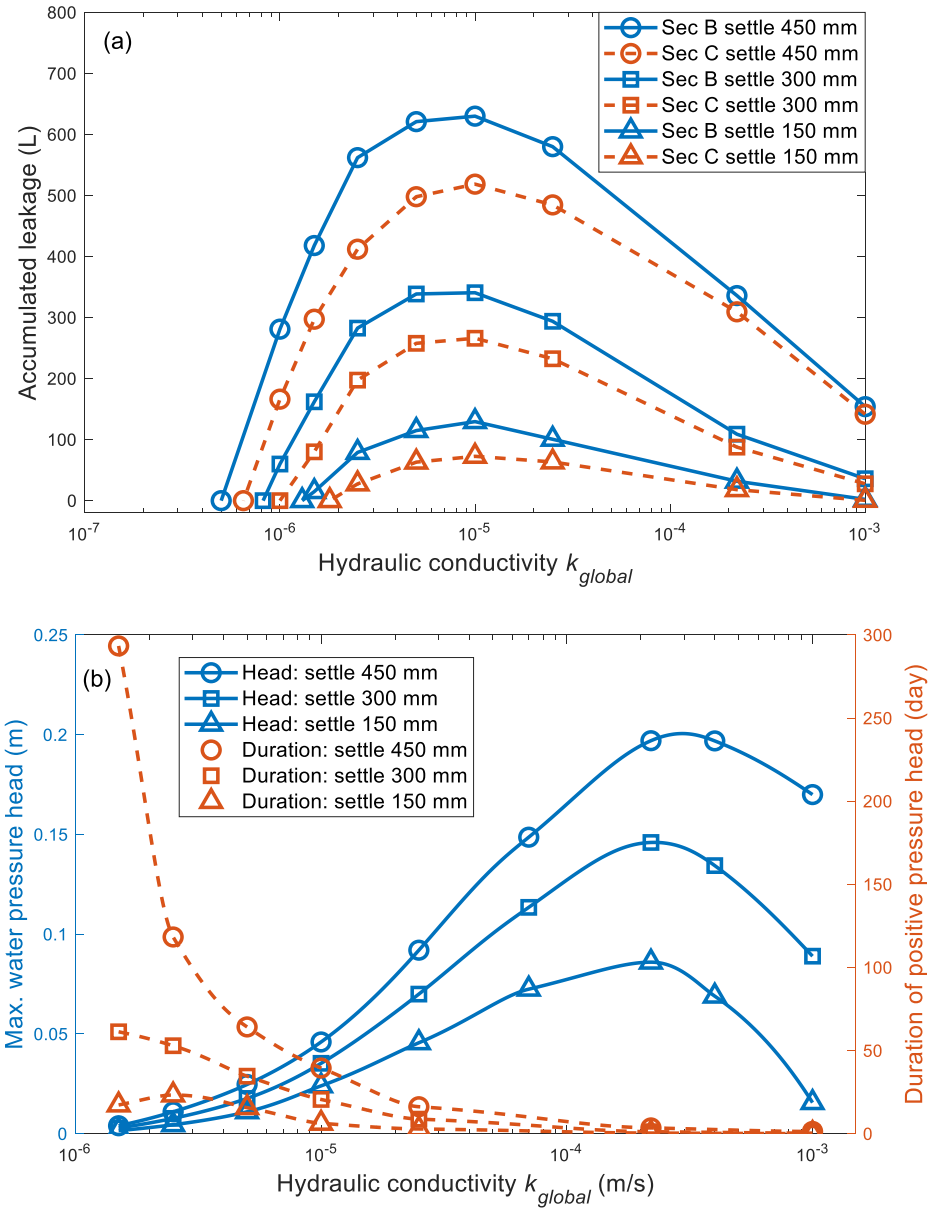

Fig. 17. Effect of soil hydraulic conductivity (k_{global}) and differential settlement depth on: (a) leakage, and (b) maximum water pressure head and duration of positive water pressure head above the hole for Section B.

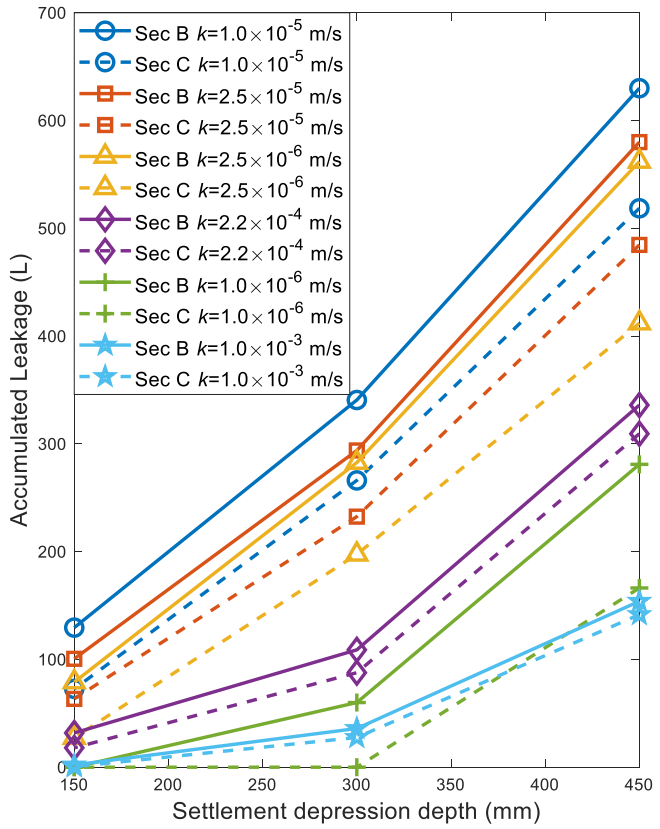

Fig. 18. Effect of settlement depression depth on leakage with different soil hydraulic conductivity (k_{global}).

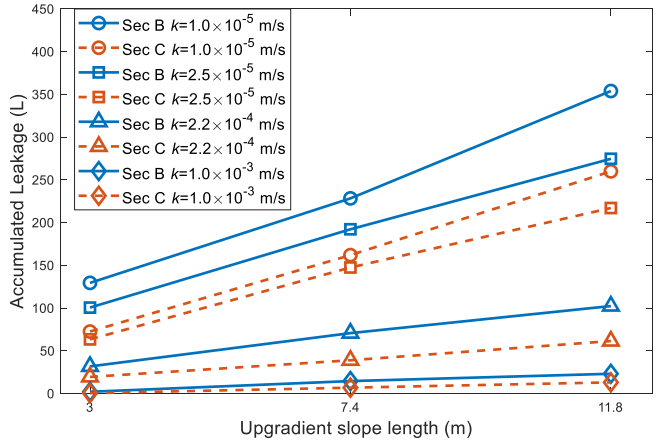

Fig. 19. Effect of upgradient slope length on leakage with different soil hydraulic conductivity (k_{global}).

× 10^{-4} m/s). This extended duration is attributed to the sand with lower k enhancing resistance to downslope flow and extending local water retention above the hole in the depression.

Analyses were also performed for cover soil with 1×10^{-7} m/s < $k_{global} \leq 1 \times 10^{-3}$ m/s) (Fig. 17a). For $1 \times 10^{-5} < k_{global} < 1 \times 10^{-3}$ m/s, leakage was almost inversely related to log(k_{global}). Conversely, for $k_{global} < 1 \times 10^{-5}$ m/s, leakage decreased as log (k_{global}) and decreased and became essentially negligible for $5 \times 10^{-7} < k_{global} < 2 \times 10^{-6}$ m/s, depending on the depth of the settlement trough. However, these results assume the soil cover is homogenous and intact. Unfortunately, for cover with $k_{global} < 1 \times 10^{-5}$ m/s, such as clay and manufactured geosynthetic clay liners (GCLs), the likelihood of desiccation cracks increases and

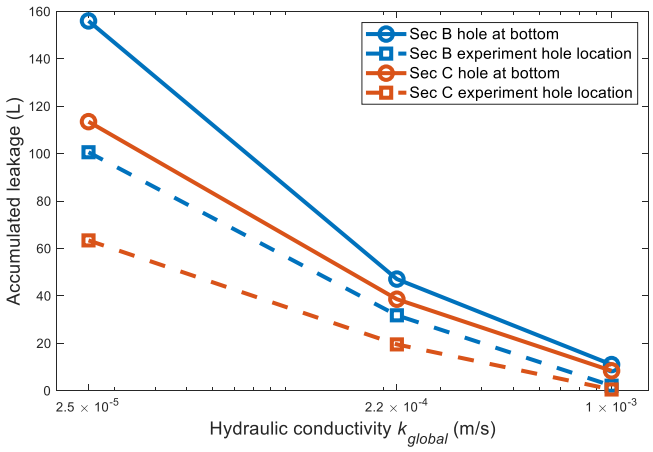

Fig. 20. Effect of hole location on leakage with different soil hydraulic conductivity (k_{global}).

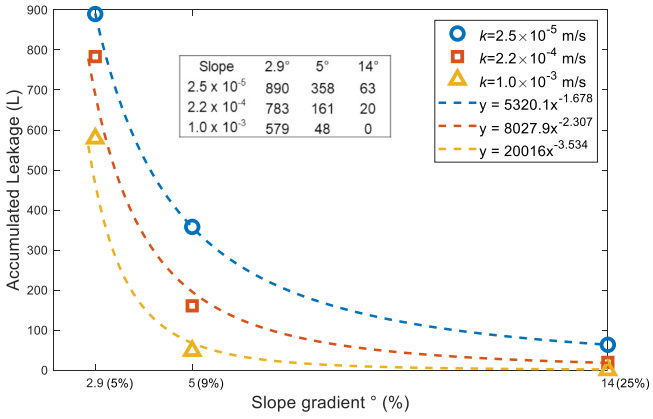

Fig. 21. Effect of slope gradient on leakage with different soil hydraulic conductivity (k_{global}) in Section C.

preferential flow through cracks or chemical interactions can become the dominant factor in increasing k_{global} and leakage (Albright et al., 2006a, 2006b; Benson et al., 2018). Specifically, with insufficient cover soil and poor selection of manufactured geosynthetic clay liners (GCLs), a loss of swelling capacity, wet-dry and/or freeze-thaw cycles and preferential bundle flow can increase the GCL hydraulic conductivity by up to 6 orders of magnitude (Bradshaw et al., 2013; Hosney and Rowe, 2014a; Hosney and Rowe, 2014b; Rowe et al., 2017a; Rowe et al., 2019; Rowe et al., 2023; Scalia IV and Benson, 2011); These phenomena with increased k_{global} are beyond the assumption and scope of this paper.

Fig. 17b illustrates that the duration of the water pressure head increases as k_{global} decreases, explaining why leakage also increases for $k_{global} < 1 \times 10^{-5}$ m/s. However, as the water pressure head starts to decrease at $k_{global} < 2.2 \times 10^{-4}$ m/s, leakage declines with decrease of k_{global} after peaking when $k_{global} \approx 1 \times 10^{-5}$ m/s. Additionally, when k_{global} drops below 5×10^{-6} m/s, increased surface runoff becomes a significant factor in reducing leakage. Specifically, for k_{global} decreases from 5×10^{-6} to 1×10^{-7} m/s, surface runoff increases from 0.5% to 82% of the total precipitation.

5.4.2. *Depth of differential settlement*

The depth of differential settlement varies depending on factors such as type of waste, water content and/or whether it is frozen when placed, uniformity of materials as placed, etc. For instance, Scalia et al. (2017) reported a 300-mm-deep differential settlement in a landfill. Therefore, understanding the impact of varying depression depths is crucial for predicting leakage levels and designing appropriate remediation

measures. Keeping all other parameters consistent for Sections B and C in period 19, increasing the settlement depth from 150 mm to 450 mm for Sections B and C significantly increases leakage (Fig. 18). The absolute difference in leakage between Sections B and C for different k_{global} is mostly stable, suggesting that the strategy of filling the surface trough becomes less effective in controlling leakage as the depression depth increases over 150 mm.

5.4.3. Upgradient slope length

In the present field experiments, the depression started only 3 m downgradient of the crest. However, differential settlement can occur anywhere along a slope. Numerical analyses demonstrated that the leakage increases approximately linearly with the distance between the crest of the slope and the depression (Fig. 19). This is because the catchment area above the depression proportionally expands as the upgradient length increases, indicating that a hole positioned lower on a slope will have a more significant impact on the leakage than one near the crest (or bench), other things being equal. The numerical results showed there is only internal flow in soil (no surface runoff) for the different upgradient slope lengths examined.

5.4.4. Location of the GMB hole

In the current experiment, the hole in the liner was 200–300 mm from the lowest contour along the depression's base in Sections B and C (Fig. 3). However, leakage is anticipated to be greater if the GMB hole is located at the lowest point of the depression, where the water head is higher. Furthermore, due to the maximum strain in areas adjacent to differential settlement (Tano et al., 2018; Villard and Briançon, 2008), the hole may naturally occur at this lowest contour.

An analysis was conducted to quantify the potential increase in leakage if the GMB hole is located at the bottom of the depression. Fig. 20 shows that, for $k = 2.2 \times 10^{-4}$ m/s, leakage in Section B increases from 31.8 L to 47.1 L, and in Section C from 19.5 L to 38.6 L if the hole moves from the original site location (referenced as "Base" in Table 6) to the bottom contour. This effect is larger at a lower $k = 2.5 \times 10^{-5}$, with leakage in both sections increasing by around 50 L when the hole is at the bottom. This indicates the potential for higher leakage in practical scenarios involving differential settlement-related defects that are located at the bottom contour. Consequently, for a cautious approach in leakage prediction, models should consider the hole to be at the lowest point of the depression.

5.4.5. Slope gradient of waste covers

The field experiment utilized a 25% (14°) slope that is widely used in waste cover designs (Stark and Newman, 2010). However, a gradient as low as 5% (2.9°) may be considered appropriate for slope stability purposes and erosion control. Thus, the effect of three common slope gradients (5%, 9% and 25%) on leakage was investigated for Section C. The numerical results indicated no surface runoff for all three cases. The other findings are summarized below.

The relationship between slope gradient (Fig. 21) and leakage could be characterized by three power law functions of the hydraulic conductivity of the cover soil. This trend is attributed to steeper slopes facilitating faster water flow downslope, reducing both the magnitude and duration of water pressure head above the hole. Notably, Fig. 21 also shows that the leakage increases much more rapidly when the slope gradient decreases to below 9%, indicating that differential settlement significantly impacts leakage on gentler slopes even when the surface trough is repaired as Section C.

6. Summary

The leakage through an 11 mm-diameter hole in a plastic liner placed on a 4H:1V slope over 15 months of monitoring of field Sections A, B and C, during which time the total precipitation was 1258 mm, has been reported and analyzed. The main observations are summarized below.

- During the 15-month study, the total leakage measured 244 L in the section with the surface trough repaired (140 mm deep; Section C) was only 43% of the 565 L observed for a similar depression that has not been backfilled (Section B).
- The relative effect of backfilling varied seasonally. In the warmer months, between June to October (2022), the section with the surface trough repaired had leakage of 55% of that in unrepaired Section B (142 L). However, this ratio decreased to 39% in the colder months (between November 2022 and March 2023; 138 L in repaired section vs 351 L in unrepaired section).

7. Conclusions

For the materials and field conditions examined, the following conclusions were reached based on the field data.

1. On a 4H:1V slope, backfilling a differential settlement trough (3 m × 2 m, depth 0.14 m) reduced leakage through a hole in the underlying geomembrane by 57%.
2. Despite lower precipitation in colder seasons, the leakage through geomembrane holes increases in those months, and filling the surface trough is particularly effective in reducing leakage.
3. Water was able to flow through the cover sand and cause leakage even when theair temperature was below freezing, because snow and sand serve as effective insulators to maintain soil temperature consistently above freezing.

The numerical results indicate the following findings.

4. The leakage through a GMB hole is inversely related to hydraulic conductivity (k) when $1 \times 10^{-5} < k < 1 \times 10^{-3}$ m/s, and directly related to k when $k < 1 \times 10^{-5}$ m/s.
5. The leakage increases significantly as the settlement depression depth increases from 150 mm to 450 mm. Filling the surface trough is less effective in controlling leakage as the depression depth increases.
6. The further down the slope a depression occurs, the greater the resulting leakage, which increases nearly linearly with the upgradient slope length of the depression
7. For a given settlement depression, the leakage through a hole in a geomembrane below that settlement depression increases with decreasing slope angle, with a significant increase in leakage if the slope gradient falls below 5°.

Data

Some or all data used are available from the corresponding author by request.

CRediT authorship contribution statement

Y.H. Fan: Writing – original draft, Validation, Investigation, Formal analysis, Data curation, Conceptualization. **R. Kerry Rowe:** Writing – review & editing, Validation, Supervision, Project administration, Methodology, Investigation, Funding acquisition, Formal analysis, Data curation, Conceptualization. **Richard W.I. Brachman:** Validation, Supervision, Methodology, Investigation, Data curation, Conceptualization. **Jamie F. VanGulck:** Writing – review & editing, Supervision, Resources, Methodology, Investigation, Funding acquisition, Formal analysis, Conceptualization.

Declaration of competing interest

The authors declare there are no competing interests.

Data availability

Data will be made available on request.

Acknowledgements

The field tests were conceived as a means of verifying and calibrating the applicability of numerical models developed with support of NSERC strategic grant STPGP 521237–18 while the fieldwork was conducted with support from the Government of the Northwest Territories.

References

Albright, W.H., Benson, C.H., Gee, G.W., Abichou, T., McDonald, E.V., Tyler, S.W., Rock, S.A., 2006a. Field performance of a compacted clay landfill final cover at a humid site. J. Geotech. Geoenviron. Eng. 132 (11), 1393–1403.
Albright, W.H., Benson, C.H., Gee, G.W., Abichou, T., Tyler, S.W., Rock, S.A., 2006b. Field performance of three compacted clay landfill covers. Vadose Zone J. 5 (4), 1157–1171.
ASTM D2487, 2011. Standard Practice for Classification of Soils for Engineering Purposes (Unified Soil Classification System). ASTM International, Conshohocken, PA, USA.
ASTM D422-63, 2007. Standard Test Method for Particle-Size Analysis of Soils. ASTM International, West Conshohocken, PA, USA.
ASTM D5084 - 16a, 2016. Standard Test Methods for Measurement of Hydraulic Conductivity of Saturated Porous Materials Using a Flexible Wall Permeameter. ASTM International, West Conshohocken, PA, USA.
Aubertin, M., Mbonimpa, M., Bussière, B., Chapuis, R., 2003. A model to predict the water retention curve from basic geotechnical properties. Can. Geotech. J. 40 (6), 1104–1122.
Benson, C.H., Thorstad, P.A., Jo, H.-Y., Rock, S.A., 2007. Hydraulic performance of geosynthetic clay liners in a landfill final cover. J. Geotech. Geoenviron. Eng. 133 (7), 814–827.
Benson, C.H., Chen, J.N., Edil, T.B., Likos, W.J., 2018. Hydraulic conductivity of compacted soil liners permeated with coal combustion product leachates. J. Geotech. Geoenviron. Eng. 144 (4).
Brachman, R.W.I., Eastman, M.K., 2013. Calculating local geomembrane indentation strains from measured radial and vertical displacements. Geotext. Geomembranes 40, 58–68.
Brachman, R.W.I., Joshi, P., Rowe, R.K., 2017. A new laboratory apparatus for measuring leakage through geomembrane holes beneath mine tailings. Can. Geotech. J. 54 (2), 147–157.
Bradshaw, S.L., Benson, C.H., Scalia, J., 2013. Hydration and cation exchange during subgrade hydration and effect on hydraulic conductivity of geosynthetic clay liners. J. Geotech. Geoenviron. Eng. 139 (4), 526–538.
Breitmeyer, R.J., Benson, C.H., Edil, T.B., 2019. Effects of compression and decomposition on saturated hydraulic conductivity of municipal solid waste in bioreactor landfills. J. Geotech. Geoenviron. Eng. 145 (4).
Bremner, H., Charpentier, C., Jacquelin, T., 2016. Case study on quality control and leak location performed on a bituminous liner mine closure project near the Arctic Circle in NWT, Canada. In: GeoAmericas- Pan-American Conference on Geosynthetics, Miami Beach. FL, USA.
Buslaev, G., Tsvetkov, P., Lavrik, A., Kunshin, A., Loseva, E., Sidorov, D., 2021. Ensuring the sustainability of Arctic industrial facilities under conditions of global climate change. Resources 10 (12), 128.
Butler, G., 2002. Nuclear power: waste management issues. Power Eng. J. 16 (4), 207–212.
Eldesouky, H., Brachman, R., 2018. Calculating local geomembrane strains from a single gravel particle with thin plate theory. Geotext. Geomembranes 46 (1), 101–110.
Fan, J., Rowe, R.K., 2022. Piping of silty sand tailings through a circular geomembrane hole. Geotext. Geomembranes 50 (1), 183–196.
Fan, Y., Brachman, R., Rowe, R., Eldesouky, H., 2021. FEM implementation of a viscoplastic model for calculating geomembrane strain due to differential settlement from degrading or thawing waste. In: Society, C.G. (Ed.), Proc. Of 74th Canadian Geotechnical Conference, Niagara, Canada.
Fan, Y., Brachman, R., Rowe, R.K., VanGulck, J.F., 2022. Design of a field test to monitor leakage through a hole in a cover geomembrane. In: Society, C.G. (Ed.), Proc. Of 75th Canadian Geotechnical Conference. Calgary, Canada.
Fan, Y.-H., Kerry Rowe, R., Brachman, R., Van Gulck, J., 2024. Impact of differential settlement on leakage through geomembranes in waste covers. Geosynth. Int. 1–42.
GeoStudio, 2021. Version 11.3.0.23668. Geo-slope international Ltd, Calgary, Alberta, Canada.
Gilson-Beck, A., 2019. Controlling leakage through installed geomembranes using electrical leak location. Geotext. Geomembranes 47 (5), 697–710.
Giroud, J., 2016. Leakage control using geomembrane liners. Soils and Rocks 39 (3), 213–235.
Giroud, J., Bonaparte, R., 1989. Leakage through liners constructed with geomembranes—part I. Geomembrane liners. Geotext. Geomembranes 8 (1), 27–67.
Giroud, J., Bonaparte, R., 2001. Geosynthetics in liquid-containing structures. In: Rowe, R.K. (Ed.), Geotechnical and Geoenvironmental Engineering Handbook. Kluwer Academic Publishing, Norwell, MA, USA, pp. 789–824.
Government of Canada, 2024. Daily precipitation data for Ontario. https://climate.weather.gc.ca/ (accessed 31 June 2024).
Hazen, A., 1893. Some physical properties of sand and gravel with special reference to the use in filtration. In: 4th Annual Report, State Board of Health. Boston.
Hopmans, J., Dane, J., 1986. Temperature dependence of soil hydraulic properties. Soil Sci. Soc. Am. J. 50 (1), 4–9.
Hosney, M.S., Rowe, R.K., 2014a. Performance of GCL after 10 Years in service in the arctic. J. Geotech. Geoenviron. Eng. 140 (10), 04014056.
Hosney, M.S., Rowe, R.K., 2014b. Performance of three GCLs used for covering gold mine tailings for 4 years under field and laboratory exposure conditions. Geosynth. Int. 21 (3), 197–212.
Keske, C.M., Mills, M., Godfrey, T., Tanguay, L., Dicker, J., 2018. Waste management in remote rural communities across the Canadian North: challenges and opportunities. Detritus 2 (1), 63.
Lide, D.R., 2005. CRC Handbook of Chemistry and Physics, 86th Edition. Taylor & Francis, Boca Raton, FL.
Maurice, R., 2002. Restauration du site minier Poirier (Joutel)–expériences acquises et suivi des travaux, Défis & Perspectives. Symposium. Economic Development Canada/Ministry of Natural Resources of Quebec/CIM, Rouyn-Noranda, Quebec, Canada.
McDougall, J.R., Fleming, I.R., Thiel, R., Dewaele, P., Parker, D., Kelly, D., 2018. Estimating degradation-related settlement in two landfill-reclaimed soils by sand-salt analogues. Waste Manag. 77, 294–303.
Nyhan, J.W., 2005. A seven-year water balance study of an evapotranspiration landfill cover varying in slope for semiarid regions. Vadose Zone J. 4 (3), 466–480.
Pandey, L.M.S., Shukla, S.K., 2020. Detection of leakage of MSW-landfill leachates through a liner defect: experimental and analytical methods. J. Geotech. Geoenviron. Eng. 146 (8).
Ramasamy, M., Power, C., Mkandawire, M., 2018. Numerical prediction of the long-term evolution of acid mine drainage at a waste rock pile site remediated with an HDPE-lined cover system. J. Contam. Hydrol. 216, 10–26.
Rowe, R.K., 1998. Geosynthetics and the minimization of contaminant migration through barrier systems beneath solid waste. In: Association, A.T. (Ed.), Proceedings of the 6th International Conference on Geosynthetics, pp. 27–103. Atlanta.
Rowe, R.K., 2005. Long-term performance of contaminant barrier systems. Geotechnique 55 (9), 631–678.
Rowe, R.K., 2012. Short- and long-term leakage through composite liners. The 7th Arthur Casagrande Lecture. Can. Geotech. J. 49 (2), 141–169.
Rowe, R.K., 2020. Protecting the environment with geosynthetics: 53rd karl terzaghi lecture. J. Geotech. Geoenviron. Eng. 146 (9), 04020081.
Rowe, R.K., Abdelatty, K., 2013. Leakage and contaminant transport through a single hole in the geomembrane component of a composite liner. Journal of geotechnical and geoenvironmental engineering 139 (3), 357–366.
Rowe, R.K., AbdelRazek, A.Y., 2019. Effect of interface transmissivity and hydraulic conductivity on contaminant migration through composite liners with wrinkles or failed seams. Can. Geotech. J. 56 (11), 1650–1667.
Rowe, R.K., Fan, J., 2021. Effect of geomembrane hole geometry on leakage overlain by saturated tailings. Geotext. Geomembranes 49 (6), 1506–1518.
Rowe, R.K., Yu, Y., 2019. Magnitude and significance of tensile strains in geomembrane landfill liners. Geotext. Geomembranes 47 (3), 439–458.
Rowe, R.K., Quigley, R.M., Brachman, R.W.I., Booker, J.R., 2004. Barrier Systems for Waste Disposal Facilities, second ed. CRC Press, Ontario, Canada.
Rowe, R.K., Brachman, R.W.I., Hosney, M.S., Take, W.A., Arnepalli, D.N., 2017a. Insight into hydraulic conductivity testing of geosynthetic clay liners (GCLs) exhumed after 5 and 7 years in a cover. Can. Geotech. J. 54 (8), 1118–1138.
Rowe, R.K., Joshi, P., Brachman, R.W.I., McLeod, H., 2017b. Leakage through holes in geomembranes below saturated tailings. J. Geotech. Geoenviron. Eng. 143 (2).
Rowe, R.K., Garcia, J., Brachman, R., Hosney, M., 2019. Chemical interaction and hydraulic performance of geosynthetic clay liners isothermally hydrated from silty sand subgrade. Geotext. Geomembranes 47 (6), 740–754.
Rowe, R.K., Garcia, J.D.D., Brachman, R.W.I., Hosney, M.S., 2023. Moisture uptake and loss of GCLs subjected to thermal cycles from silty sand subgrade. Geosynth. Int. 30 (2), 113–128.
Scalia, J., Benson, C.H., Albright, W.H., Smith, B.S., Wang, X., 2017. Properties of barrier components in a composite cover after 14 Years of service and differential settlement. J. Geotech. Geoenviron. Eng. 143 (9), 1–11.
Scalia IV, J., Benson, C.H., 2011. Hydraulic conductivity of geosynthetic clay liners exhumed from landfill final covers with composite barriers. J. Geotech. Geoenviron. Eng. 137 (1), 1–13.
Stark, T., Newman, E., 2010. Design of a landfill final cover system. Geosynth. Int. 17 (3), 124–131.
Stohr, C., Su, W.-J., Follmer, L., DuMontelle, P., Griffin, R., 1988. Engineering geology investigations of a hazardous-waste landfill in West Central Illinois, USA. Bull. Eng. Geol. Environ. 37 (1).
Subbotin, A., Kravchenko, A., Dmitrienko, A., 2022. Improving the efficiency of foundation construction in permafrost conditions on the example of the use of geopolymer materials. In: Journal of Physics: Conference Series. IOP Publishing, 012122.
Take, W., Rowe, R., Brachman, R., Arnepalli, D., 2015. Thermal exposure conditions for a composite liner with a black geomembrane exposed to solar radiation. Geosynth. Int. 22 (1), 93–109.
Tano, B.F.G., Stoltz, G., Coulibaly, S.S., Bruhier, J., Dias, D., Olivier, F., Touze-Foltz, N., 2018. Large-scale tests to assess the efficiency of a geosynthetic reinforcement over a cavity. Geosynth. Int. 25 (2), 242–258.
Touze-Foltz, N., Xie, H., Stoltz, G., 2021. Performance issues of barrier systems for landfills: a review. Geotext. Geomembranes 49 (2), 475–488.

Van Genuchten, M.T., 1980. A closed-form equation for predicting the hydraulic conductivity of unsaturated soils. Soil Sci. Soc. Am. J. 44 (5), 892–898.
Villard, P., Briançon, L., 2008. Design of geosynthetic reinforcements for platforms subjected to localized sinkholes. Can. Geotech. J. 45 (2), 196–209.
Warith, M., Smolkin, P., Caldwell, J., 1994. Evaluation of an HDPE geomembrane landfill cover performance. Geosynth. Int. 1 (2), 201–219.
Weeks, B., Wilson, G.W., 2005. Variations in moisture content for a soil cover over a 10 year period. Can. Geotech. J. 42 (6), 1615–1630.
Williams, D., 2008. The influence of climate on seepage from mine waste storages during deposition and post-closure, Mine Closure 2008. In: Proceedings of the Third International Seminar on Mine Closure. Australian Centre for Geomechanics, pp. 461–473.
Wilson, G., Machibroda, R., Lee Barbour, S., Woyshner, M., 1993. Modelling of soil evaporation from waste disposal sites. In: Proceedings of the Joint CSCE-ASCE National Conference on Environmental Engineering, pp. 281–288. Montreal.
Xie, H., Xu, W., Wang, L., Yan, H., Wu, J., 2023. Equivalent analytical models for assessment of landfill composite liners. Geosynth. Int. 1–35.
Xu, Y., Xue, X., Dong, L., Nai, C., Liu, Y., Huang, Q., 2018. Long-term dynamics of leachate production, leakage from hazardous waste landfill sites and the impact on groundwater quality and human health. Waste Manag. 82, 156–166.
Zhang, J., Zhang, J.-m., Xing, B., Liu, G.-d., Liang, Y., 2021. Study on the effect of municipal solid landfills on groundwater by combining the models of variable leakage rate, leachate concentration, and contaminant solute transport. J. Environ. Manag. 292, 112815.
Zhu, M., Geotechnical and wind performance of engineered turf landfill cover, Proceedings of Sessions of Geo-Extreme 2021. Geo-Institute of ASCE, Savannah, Georgia, pp. 236-245.